https://doi.org/10.1093/nar/gkac485

TWIST1 methylation by SETD6 selectively antagonizes LINC-PINT expression in glioma

Lee Admoni-Elisha[1,2], Tzofit Elbaz[1,2], Anand Chopra[3], Guy Shapira[4,5], Mark T. Bedford[6], Christopher J. Fry[7], Noam Shomron[4,5], Kyle Biggar[3], Michal Feldman[1,2] and Dan Levy[1,2,*]

[1]The Shraga Segal Department of Microbiology, Immunology and Genetics, Faculty of Health Sciences, Ben-Gurion University of the Negev, 84105 Be'er-Sheva, Israel, [2]National Institute for Biotechnology in the Negev, Ben-Gurion University of the Negev, P.O.B. 653, Be'er-Sheva 84105, Israel, [3]Carleton University, 1125 Colonel By Drive, Ottawa, Ontario K1S 5B6, Canada, [4]Faculty of Medicine, Tel Aviv University, Tel Aviv, Israel, [5]Edmond J. Safra Center for Bioinformatics, Tel Aviv University, Tel Aviv, Israel, [6]Department of Carcinogenesis, M.D. Anderson Cancer Center, Houston, TX, USA and [7]Cell Signaling Technology Inc., Danvers, MA, USA

Received October 27, 2021; Revised May 16, 2022; Editorial Decision May 18, 2022; Accepted May 30, 2022

ABSTRACT

Gliomas are one of the most common and lethal brain tumors among adults. One process that contributes to glioma progression and recurrence is the epithelial to mesenchymal transition (EMT). EMT is regulated by a set of defined transcription factors which tightly regulate this process, among them is the basic helix-loop-helix family member, TWIST1. Here we show that TWIST1 is methylated on lysine-33 at chromatin by SETD6, a methyltransferase with expression levels correlating with poor survival in glioma patients. RNA-seq analysis in U251 glioma cells suggested that both SETD6 and TWIST1 regulate cell adhesion and migration processes. We further show that TWIST1 methylation attenuates the expression of the long-non-coding RNA, LINC-PINT, thereby promoting EMT in glioma. Mechanistically, TWIST1 methylation represses the transcription of LINC-PINT by increasing the occupancy of EZH2 and the catalysis of the repressive H3K27me3 mark at the LINC-PINT locus. Under un-methylated conditions, TWIST1 dissociates from the LINC-PINT locus, allowing the expression of LINC-PINT which leads to increased cell adhesion and decreased cell migration. Together, our findings unravel a new mechanistic dimension for selective expression of LINC-PINT mediated by TWIST1 methylation.

INTRODUCTION

Gliomas are the most common brain tumors among adults, representing 81% of malignant brain tumors (1,2). Although it accounts for <1% of all newly diagnosed cancers, gliomas are one of the cancers with the highest mortality rates (3). Gliomas originate from the glial tissue (2,4) and are classified according to histopathological characteristics. Low grade gliomas include oligodendroglioma and astrocytoma, while grade III gliomas are anaplastic oligodendroglioma and astrocytoma (1,4). Grade IV is also known as glioblastoma (GBM). GBMs are the most aggressive malignant brain tumor with a median survival of 1–2 years and an overall 5-years-survival rate of 5% (5,6)

One process that contributes to glioma progression and recurrence is the epithelial to mesenchymal transition (EMT) (7–9). In this process, epithelial cells undergo multiple changes which include loss of their junctions and apical-basal polarity, cytoskeleton reorganization and increased production of extracellular matrix (ECM) components (10,11). These changes result in enhanced motility, invasiveness, and resistance to apoptosis (12). EMT is regulated by a set of defined transcription factors (TFs), including TWIST1, SNAIL, SLUG and ZEB1/2 (10,12). Indeed, these TFs were found to play a key role in the development and progression of glioma (13–17).

TWIST1 belongs to the bHLH (basic helix-loop-helix) transcription factors. The human TWIST1 is ∼21 kDa and contains two nuclear localization sequences (18). TWIST1 binds the DNA sequences $^{5'}$CANNTG^{3}, named E-boxes, through a conserved bHLH domain. This domain is also important for the interactions with other proteins to form homo- and hetero-dimeric complexes (18,19).

In addition to the physiologic role of TWIST1 in embryonic development, organogenesis and angiogenesis (18,20), this transcription factor is also associated with many types of aggressive tumors (18,21). The most critical pathological function of TWIST1 in cancer is facilitating tumor invasion and metastasis by promoting EMT (22). TWIST1 is highly expressed in tissue specimens of glioma patients (23). TWIST1 was also found to promote invasion in glioma through the upregulation of genes such as SNAI1, MMP2,

*To whom correspondence should be addressed. Tel: +972 8 647 7251; Email: ledan@post.bgu.ac.il

© The Author(s) 2022. Published by Oxford University Press on behalf of Nucleic Acids Research.
This is an Open Access article distributed under the terms of the Creative Commons Attribution-NonCommercial License (http://creativecommons.org/licenses/by-nc/4.0/), which permits non-commercial re-use, distribution, and reproduction in any medium, provided the original work is properly cited. For commercial re-use, please contact journals.permissions@oup.com

Downloaded from https://academic.oup.com/nar/advance-article/doi/10.1093/nar/gkac485/6606173 by Ben Gurion University of the Negev-Medical Library user on 15 June 2022

HGF and FN1, which associate with adhesion, extracellular matrix, cell motility and locomotion.

TWIST1 is regulated by diverse post-translational modifications. Phosphorylation at S68 promotes the heterodimerization with E12, which leads to a pro-invasive phenotype (24) and prevents its ubiquitination-mediated degradation (25). In contrast, AKT1 and AKT2 phosphorylate TWIST1 at S42, a modification promoting TWIST1 degradation (26). Upon DNA damage, RNF8 mediates K63-linked poly-ubiquitination at K38, leading to TWIST1 stabilization and activation (27). In lung cancer, PRMT1 modulates TWIST1 function through methylation at R34. This methylation was shown to be crucial for the repression of epithelial markers and TWIST1 nuclear localization (28). TWIST1 function is also regulated by di-acetylation at K73 and K76 mediated by the acetyltransferase Tip60. This di-acetylation promotes the TWIST1- BRD4 interaction which activates the transcription of WNT5a (29). Up to date, the regulation of TWIST1 activity by lysine methylation has not been reported yet.

Lysine methylation is catalyzed by protein-lysine methyltransferases. While extensive studies were performed on histone proteins, it is now clear that lysine methylation extends far beyond that, with nearly 3000 non-histone sites reported to be methylated in PhosphoSitePlus (30). However, only a small fraction of these methylation events was functionally studied. The SET domain-containing protein 6 (SETD6) is a member of the lysine methyltransferase family. SETD6 was first enzymatically characterized as a regulator of inflammation through the methylation of NF-κB/RelA protein (31). Later studies revealed its role in a variety of cellular processes and signaling pathways such as transcription, WNT signaling, cell cycle, oxidative stress response, hormone receptor signaling and more (32–36).

Long non-coding RNAs (LncRNAs) are a large heterogeneous group of RNA molecules longer than 200 nucleotides that are not transcribed into functional proteins. Despite not being transcribed, it is now apparent that LncRNAs are functional molecules that regulate diverse cellular processes (37). Long intergenic p53 induced transcript (LINC-PINT) was first characterized as a target of P53 in mouse cell line, which regulates gene expression through interaction with the Polycomb repressive complex 2 (PRC2) (38). Later studies have shown that LINC-PINT inhibits pro-invasive genes and abolishes the invasiveness of cancer cells (39). Accordingly, LINC-PINT was found to be downregulated in multiple types of cancer such as colorectal cancer, lung adenocarcinoma and GBM (39,40). Recently, a connection between LINC-PINT to EMT was identified. In GBM, LINC-PINT was found to suppress EMT phenotype by blocking the WNT/β-catenin pathway (40), and in laryngeal squamous cell carcinoma it was found to suppress EMT by inhibiting the transcription factor ZEB1 (41).

Here, we show that TWIST1 is regulated by lysine methylation. We have found that TWIST1 is targeted for methylation at chromatin by SETD6 and that high expression of SETD6 correlates with poor survival in glioma patients. RNA-seq experiments in U251 SETD6 depleted cells as well as cells stably expressing TWIST1, revealed a significant enrichment in cellular processes linked to extracellular matrix organization and cell adhesion which are involved in the EMT process during tumorigenesis (42). Our data further provides evidence that the methylation of TWIST1 at K33 selectively regulates the expression of LINC-PINT. Methylated TWIST1 binds to the LINC-PINT locus and limits it transcription by increasing the repressive H3K27me3 mark. The occupancy of unmethylated TWIST1 at the LINC-PINT locus is dramatically reduced and correlates with increased expression of LINC-PINT RNA, resulting in augmented cell adhesion and reduced cell migrations, thereby mimicking the phenotypes of over-expressed LINC-PINT in glioma cells.

MATERIALS AND METHODS

Plasmids

For recombinant purification TWIST1, SNAIL and SLUG sequences were amplified by PCR and subcloned into pET-Duet plasmids. TWIST1 mutants were generated using site-directed mutagenesis and cloned into pET-Duet. Primers used for cloning and mutagenesis are listed in Table 1. TWIST1 WT and K33R were further cloned into pcDNA3.1 3xFLAG. SETD6 was cloned into pcDNA3.1 3xHA plasmid. For viral infection, TWIST1 WT and K33R were cloned into pWZL-FLAG plasmid. pBABE plasmid containing LINC-PINT cDNA (BC130416.1) were kindly provided by Dr. Maite Huarte (University of Navarra, Spain). For CRISPR/Cas9 SETD6 knock-out, four different gRNAs for SETD6 were cloned into lentiCRISPR plasmid (Addgene, #49535). For stable transfection pWZL constructs (Empty, FLAG TWIST1 WT, FLAG TWIST1 K33R) or pBABE (LINC-PINT) were used.

Cell lines, transfection, infection and treatment

Human glioma cell line U251, Human embryonic kidney cells (HEK293T) were maintained in Dulbecco's modified Eagle's medium (Sigma, D5671) with 10% fetal bovine serum (FBS) (Gibco), penicillin-streptomycin (Sigma, P0781), 2 mg/ml L-glutamine (Sigma, G7513) and non-essential amino acids (Sigma, M7145), at 37°C in a humidified incubator with 5% CO_2.

Cell transfections were performed using polyethyleneimine (PEI) reagent (Polyscience Inc., 23966) or jetPRIME (Polyplus transfection, 114-07) according to manufacturer's protocol.

For CRISPR/Cas9 SETD6 knock-out, four different gRNAs for SETD6 were cloned into lentiCRISPR plasmid. Following transfection and puromycin selection (2.5μg/ml), single clones were isolated, expanded and validated by sequencing. LentiCRISPR plasmid with no gRNAs was used as control.

For stable transfections in U251 cell line, retroviruses were produced by transfecting HEK293T cells with the indicated pWZL constructs (Empty, FLAG TWIST1 WT, FLAG TWIST1 K33R) or pBABE (LINC-PINT) with plasmids encoding VSV and gag-pol. U251 cells were transduced with the viral supernatants and selected with 500 μg/ml hygromycin B (TOKU-E).

Downloaded from https://academic.oup.com/nar/advance-article/doi/10.1093/nar/gkac485/6606173 by Ben Gurion University of the Negev-Medical Library user on 15 June 2022

Table 1. Primers for cloning and mutagenesis

Name	Sequence 5′ to 3′
TWIST1 WT FW	GGCGGCGCGCCCAGGACGTGTCCAGCTCGC
TWIST1 WT Rev	GGCTTAATTAACTAGTGGGACGCGGACATGG
SLUG FW	GGCGGCGCGCCCCGCGCTCCTTCCTGGTC
SLUG Rev	GGCTTAATTAATCAGTGTGCTACACAGCAGCC
SNAIL FW	GGCGGCGCGCCCCGCGCTCTTTCCTCGTCAG
SNAIL Rev	GGCTTAATTAATCAGCGGGGACATCCTGAGC
TWIST1 K33R FW	CAGCAGCCGCCGAGCGGCAGGCGCGGGGGACGCAA
TWIST1 K33R Rev	GCTTGCGTCCCCCGCGCCTGCCGCTCGGCGGCTGC
TWIST K73R FW	GCCCGGCCCAGGGCAGGCGCGGCAAGAAGTCTGC
TWIST K73R Rev	CAGACTTCTTGCCGCGCCTGCCCTGGGCCGGGCTGC

Recombinant proteins and peptides

Escherichia coli Rosetta transformed with a plasmid expressing His tagged TWIST1 WT or mutants, SNAIL, SLUG were grown in LB medium. Bacteria were harvested by centrifugation after IPTG induction (0.1 mM IPTG, 18° ON) and lysed (Lysis buffer: PBS, 10 mM Imidazole, 1 mM PMSF, 0.1% triton, cOmplete Mini protease inhibitor tablet) by sonication on ice (25% amplitude, 1 min total, 10/5 s ON/OFF). His-tagged proteins were purified using Ni-NTA beads (Pierce) or on a HisTrap column (GE) with the ÄKTA gel filtration system. Proteins were eluted by 0.5 M imidazole followed by dialysis to 10% glycerol in phosphate-buffered saline (PBS). Recombinant GST SETD6 was expressed and purified as previously described (31).

Antibodies, western blot analysis and immunoprecipitation

Primary antibodies used were: anti-FLAG (Sigma, F1804), anti-HA (Millipore, 05–904), anti-Actin (Abcam, ab3280), anti-mono-methyl lysine (Cell Signaling, 14679), anti-GST (Abcam, ab9085), anti-SETD6 (Genetex, GTX629891), anti-TWIST1 (Abcam 50887), anti-His (Thermo Fisher scientific, rd230540a), anti-EZH2 (Cell Signaling #5246) anti H3K27me3 (Cell Signaling, 9733) and anti- histone3 (H3) (Abcam, ab10799). Anti-TWIST1 K33me1 were generated in collaboration with Cell Signaling Technology. Rabbits were immunized with a synthetic peptide corresponding to residues surrounding mono-methylated Lys33 of human TWIST1 protein. The antibodies were purified by peptide affinity chromatography. A total of 8 antibodies were generated and the two antibodies that showed the highest specificity toward TWIST1 K33me1 were used. HRP-conjugated secondary antibodies, goat anti-rabbit, goat anti-mouse, were purchased from Jackson ImmunoResearch (111-035-144, 115-035-062 respectively). For Western blot analysis, cells were homogenized and lysed in RIPA buffer (50 mM Tris–HCl pH 8, 150 mM NaCl, 1% Nonidet P-40, 0.5% sodium deoxycholate, 0.1% SDS, 1 mM DTT and 1:100 protease inhibitor mixture (Sigma)). Samples were resolved on SDS- PAGE, followed by western blot analysis. For immunoprecipitation, proteins extracted from cells were incubated overnight at 4°C with FLAG-M2 beads (Sigma, A2220) or pre- conjugated A/G agarose beads (Santa Cruz, SC-2003) with antibody of interest. The beads were then washed three times with RIPA buffer and submitted to SDS-PAGE and western blot analysis.

In-vitro methylation assay

Methylation assay reactions contained 1 μg of His-TWIST1 WT or mutant and 4 μg of His SETD6 or GST SETD6, 2 mCi of 3H-labeled *S*-adenosyl-methionine (SAM) (Perkin-Elmer, AdoMet) and PKMT buffer (20 mM Tris–HCl pH 8, 10% glycerol, 20 mM KCl, 5 mM $MgCl_2$). The reaction tubes were incubated overnight at 30°C. The reactions were resolved by SDS-PAGE for Coomassie staining (Expedeon, InstantBlue) or autoradiography.

For the non-radioactive (cold) methylation assay, 300 μM non-radioactive SAM was added (Abcam, ab142221).

Semi *In-vitro* methylation assay

HEK293T cells were transfected with FLAG-TWIST1 WT or K33R plasmids. Chromatin fractions were immunoprecipitated with FLAG-M2 beads overnight at 4°C. The samples were then washed 3 times with dilution buffer and once with PKMT buffer, followed by an *in-vitro* radioactive methylation assay overnight at 30°C, in the presence of 4 μg His-SETD6. The reactions were resolved by SDS-PAGE for Coomassie staining or autoradiography.

Enzyme-linked immunosorbent assay (ELISA)

Approximately 2ug of His-TWIST1, His-SNAIL, His-SLUG or BSA diluted in PBS were added to a 96-well plate (Greiner Microlon) and incubated for 1 h at room temperature followed by blocking with 3% BSA for 30 min. Then, the plate was covered with 0.5 μg GST-SETD6 or GST protein (negative control) diluted in 1% BSA in PBST for 1 h at room temperature. Plates were then washed and incubated with primary antibody (anti-GST, 1:4000 dilution) followed by incubation with HRP-conjugated secondary antibody (goat anti-rabbit, 1:2000 dilution) for 1 h. Finally, TMB reagent and then 1 N H_2SO_4 were added; the absorbance at 450 nm was detected using Tecan Infinite M200 plate reader.

ECM adhesion assay

For cell adhesion assay, cells were serum starved (0% FBS) overnight. Then, cells were harvested and 1×10^5 cells/well were plated on a fibronectin (Millipore, 341631) or collagen I (R&D systems, 3440) (pre-coated 96-well plate (2.5 μg/well) or BSA as a negative control (5% in PBS) for 4 h, followed by a PBS wash and crystal violet staining (0.5% crystal violet in 20% methanol). Crystal violet staining was solubilized in 2% SDS and quantified at 550 nm using Tecan Infinite M200 plate reader.

Downloaded from https://academic.oup.com/nar/advance-article/doi/10.1093/nar/gkac485/6606173 by Ben Gurion University of the Negev-Medical Library user on 15 June 2022

Table 2. Primers for qPCR and ChIP qPCR

Name	Sequence 5′ to 3′
GAPDH FW	AGCCACATCGCTCAGACAC
GAPDH Rev	GCCCAATACGACCAAATCC
LINC-PINT Exon 1 FW (qPCR)	AAGGGATGGGACCAGAGAGA
LINC-PINT Exon 1 Rev (qPCR)	TCAGGAAGTGAGGTACGGAGA
LINC-PINT Exon 3 FW (qPCR)	GGGATAATTTGCCATCTGGA
LINC-PINT Exon 3 Rev (qPCR)	CCGTTTCTTCCATTTTCCTCT
LINC-PINT BS1 FW (ChIP)	CTGCTCGGCTCAGAACTCGG
LINC-PINT BS1 Rev (ChIP)	CAGGCCCTATGTGGATGTGGG
LINC-PINT BS2 FW (ChIP)	CCCTAGTCAGTGACCCAGAAGG
LINC-PINT BS2 Rev (ChIP)	CAGGGCAGAGACACCAATACAGAG
LINC-PINT- EZH2/H3K27me3 BS FW (ChIP)	CGCCAGGCTAGAGCACAG
LINC-PINT- EZH2/H3K27me3 BS Rev (ChIP)	CCATCCTGGCGAACATGG

Wound healing migration assay

For migration assay, 1×10^5 cells were seeded in 24-well plates 1 day before performing the wound. The wound was produced using 200 ul pipette tip. Cell migration was monitored for 48 h, following image processing and wound closure analysis by LionheartTM FX Automated Microscope (4×).

RNA Extraction and real-time qPCR

Total RNA was extracted using the NucleoSpin RNA Kit (Macherey-Nagel). 200 ng of the extracted RNA was reverse-transcribed to cDNA using the iScript cDNA Synthesis Kit (Bio-Rad) according to the manufacturer's instructions. Real-time qPCR was performed using the UPL probe library system or SYBR green I master (Roche) in a LightCycler 480 System (Roche). The real-time qPCR primers were designed using the universal probe library assay design center (Roche) and UCSC Genome browser (Table 2). All samples were amplified in triplicates in a 384-well plate using the following cycling conditions: 10 min at 95°C, 45 cycles of 10 s at 95°C, 30 s at 60°C and 1 s at 72°C, followed by 30 s at 40°C. Gene expression levels were normalized to GAPDH and controls of the experiment.

Chromatin extraction

Cells were cross-linked using 1% formaldehyde (Sigma) added directly to the medium and incubated on a shaking platform for 10 min at room temperature. The cross-linking reaction was stopped by adding 0.125 M glycine for 5 min. Cells were harvested and washed twice with PBS and then lysed in 1 ml cell lysis buffer (20 mM Tris–HCl pH 8, 85 mM KCl, 0.5% Nonidet P-40, 1:100 protease inhibitor cocktail) for 10 min on ice. Nuclear pellets were resuspended in 200 μl nuclei lysis buffer (50 mM Tris–HCl pH 8, 10 mM EDTA, 1% SDS, 1:100 protease inhibitor cocktail) for 10 min on ice, and then sonicated (Bioruptor, Diagenode) at high power settings for 3 cycles, 6 min each (30 s ON/OFF). Samples were centrifuged (20 000*g*, 15 min, 4°C) and the soluble chromatin fraction was collected. In some experiments, a Micrococal-Chromatin extraction protocol was used: cells were harvested and resuspended in Buffer A (10 mM HEPES pH 7.9, 10 mM KCl, 1.5 mM $MgCl_2$, 0.34 M sucrose and 10% glycerol) supplemented with 0.1% triton X-100, 1 mM DTT, 1:200 protease inhibitor mixture (PI) and 100 nM PMSF (Sigma). Cells were incubated for 8 min on ice, then centrifuged 5 min at 1850*g,* 4°C. The pellet was washed once with Buffer A supplemented with DTT, PI and PMSF, then lysed with Buffer B (3 mM EDTA and 0.2 mM EGTA) supplemented with DTT and PI, for 30 min on ice. Samples were centrifuged 5 min at 1850*g,* 4°C to pellet the chromatin fraction. Finally, chromatin fraction was solubilized in Buffer A with 1:100 micrococcal nuclease enzyme (NEB) and incubated for 15 min at 37°C shaker.

For protein-protein interaction analysis, the soluble chromatin was precleared with Magna ChIP™ Protein A + G Magnetic Beads (Millipore, 16-663) for 1 h and then incubated overnight at 4°C with magnetic FLAG-M2 beads. The immunoprecipitated complexes were washed once with TSE150 buffer [20 mM Tris–HCl (pH 8), 2 mM EDTA, 1% Triton X-100, 0.1% SDS and 150 mM NaCl], TSE500 buffer [20 mM Tris–HCl (pH 8), 2 mM EDTA, 1% Triton X-100, 0.1% SDS and 500 mM NaCl], buffer 3 [250 mM LiCl, 10 mM Tris–HCl (pH 8), 1 mM EDTA, 1% sodium deoxycholate, and 1% Nonidet P-40], and twice with TE buffer [10 mM Tris–HCl (pH 8) and 1 mM EDTA]. Immunoprecipitated complexes were resolved in protein sample buffer and analyzed by Western blot.

Chromatin immunoprecipitation (ChIP)-qPCR and

The chromatin fraction was diluted 5× in dilution buffer [20 mM Tris–HCl (pH 8), 2 mM EDTA, 150 mM NaCl, 1.84% Triton X-100 and 0.2% SDS]. Chromatin was precleared overnight at 4°C with A + G magnetic beads. The precleared sample was then immunoprecipitated with magnetic FLAG-M2 beads or A/G magnetic beads preconjugated with the indicated antibody. The immunoprecipitated complexes were washed according to the chromation extraction protocol detailed above. DNA was eluted with elution buffer (50 mM $NaHCO_3$, 140 mM NaCl and 1% SDS) containing ribonuclease A (0.2 μg/μl) and proteinase K (0.2 μg/μl). Last, the DNA eluates were de-cross-linked at 65°C overnight with shaking at 900 rpm and purified by NucleoSpin Gel and PCR Clean-up kit (Macherey-Nagel), according to the manufacturer's instructions. Purified DNA was subjected to qPCR using specific primers (Table 2). Primers for TWIST1 binding sites were designed based on H3K4me3, H3K27Ac and TF clusters in LINC-PINT locus and the occurrence of E-box elements ($^{5'}$CANNTG$^{3'}$). Primers for EZH2 and H3K27me3 binding sites were de-

Downloaded from https://academic.oup.com/nar/advance-article/doi/10.1093/nar/gkac485/6606173 by Ben Gurion University of the Negev-Medical Library user on 15 June 2022

signed using ChIP-seq data previously published (43,44) and viewed using Integrated Genomics Viewer software (45). qPCR was performed using SYBR Green I Master (Roche) in a LightCycler 480 System (Roche). All samples were amplified in triplicates in a 384-well plate using the following cycling conditions: 5 min at 95°C, 45 cycles of amplification; 10 s at 95°C, 10 s at 60°C, and 10 s at 72°C, followed by melting curve acquisition; and 5 s at 95°C, 1 min at 65°C and monitoring up to 97°C, and lastly cooling for 30 s at 40°C. The results were normalized to input DNA and presented as % input.

Mass spectrometry

Sample of non-radioactive methylation assay containing 2 μg His-TWIST1 and 4μg GST SETD6 were incubated with 3.2 mM SAM overnight at 30°C. An additional sample without SAM served as reference. For sample preparation (Weizmann Institute of Science), proteins were reduced with 5 mM dithiothreitol (Sigma) for 1 h at room temperature and alkylated with 10 mM iodoacetamide (Sigma) in the dark for 45 min at room temperature. Proteins were then subjected to digestion with trypsin (Promega; Madison, WI, USA) overnight at 37°C at 50:1 protein:trypsin ratio, followed by a second trypsin digestion for 4 h. The digestions were stopped by addition of trifluroacetic acid (1% final concentration). Following digestion, peptides were desalted using Oasis HLB, μElution format (Waters, Milford, MA, USA). The samples were vacuum dried and stored in –80˚C until further analysis. ULC/MS grade solvents were used for all chromatographic steps. Each sample was loaded using split-less nano-Ultra Performance Liquid Chromatography (10 kpsi nanoAcquity; Waters, Milford, MA, USA). The mobile phase was: A) H_2O + 0.1% formic acid and B) acetonitrile + 0.1% formic acid. Desalting of the samples was performed online using a reversed-phase Symmetry C18 trapping column (180 μm internal diameter, 20 mm length, 5 μm particle size; Waters). The peptides were then separated using a T3 HSS nano-column (75 μm internal diameter, 250 mm length, 1.8 μm particle size; Waters) at 0.35 μl/min. Peptides were eluted from the column into the mass spectrometer using the following gradient: 4–30% B in 50 min, 30–90% B in 5 min, maintained at 90% for 5 min and then back to initial conditions. The nanoUPLC was coupled online through a nanoESI emitter (10 μm tip; New Objective; Woburn, MA, USA) to a quadrupole orbitrap mass spectrometer (Q Exactive Plus, Thermo Scientific) using a FlexIon nanospray apparatus (Proxeon). Data was acquired in data dependent acquisition (DDA) mode, using a Top20 method. MS1 resolution was set to 70 000 (at 400 m/z), mass range of 300–1650 m/z, AGC of 3e6 and maximum injection time was set to 20 ms. MS2 resolution was set to 17 500, quadrupole isolation 1.7 m/z, AGC of 1e6, dynamic exclusion of 30 s and maximum injection time of 60 ms. Data was analysed using Byonic search engine (Protein Metrics) against the Human protein database (SwissProt Dec20) allowing for the following modifications: fixed carbamidomethylation on C, variable protein N-terminal acetylation, oxidation on M, deamidation on NQ, methylation on K, dimethylation on K and trimethylation on K. Protein FDR was set to 1%.

RNA-seq and data processing

Total RNA was extracted from U251 cells (SETD6 control versus KO or Empty versus TWIST1 WT) using the NucleoSpin RNA Kit (Macherey-Nagel). Samples were prepared in triplicates (SETD6 KO) or duplicates (TWIST1-WT cells). RNA-seq libraries were prepared at the Crown Genomics institute of the Nancy and Stephen Grand Israel National Center for Personalized Medicine, Weizmann Institute of Science. Libraries were prepared using the INCPM-mRNA-seq protocol. Briefly, the polyA fraction (mRNA) was purified from 500 ng of total input RNA followed by fragmentation and the generation of double-stranded cDNA. After Agencourt Ampure XP beads cleanup (Beckman Coulter), end repair, A base addition, adapter ligation and PCR amplification steps were performed. Libraries were quantified by Qubit (Thermo fisher scientific) and TapeStation (Agilent). Sequencing was done on a Hiseq instrument (Illumina) using two lanes of an SR60_V4 kit, allocating 20M reads per sample (single read sequencing).

Data processing of SETD6 KO RNA-seq: Adaptor removal and bad quality filtering was performed using Trimmomatic-0.32. Reads were than mapped to the human genome version GRCh38 using STAR-2.3.0. Counting was done using HTSeq-count version 0.6.1. (46). Statistical analysis was done using the DESeq2 R package while normalized counts were generated using the vsd function.

Data processing for TWIST1 U251 RNA-seq: PolyA/T stretches and Illumina adapters were trimmed from the reads using cutadapt (DOI: https://doi.org/10.14806/ej.17.1.200); resulting reads shorter than 30bp were discarded. Reads were mapped to the Homo Sapiens GRCh38 reference genome using STAR (47), supplied with gene annotations downloaded from Ensembl (and with EndToEnd option and outFilterMismatchNoverLmax was set to 0.04). Expression levels for each gene were quantified using htseq-count (46), using the gtf above. TPM values were estimated independently using Kallisto (48). Raw gene counts were normalized and compared using DESeq 2 1.23.0 (49). Differentially expressed genes (P-adj < 0.05) were then subjected to hierarchical clustering using Heatmapper web tool (50).

Bioinformatic analysis

SETD6 expression levels analysis was performed based on the REMBRANDT dataset (51), Kaplan-Meier survival analyzes were generated using the CGGA (52), REMBRANDT, and TCGA (https://www.cancer.gov/tcga) databases. Gene correlation analysis was performed based on the CGGA database. All data was extracted from the GlioVis data portal (53). For SETD6 control vs. KO experiment, Gene set enrichment analysis (54,55) of all genes was performed for Hallmark gene sets. SETD6 and TWIST1 shared target genes were analyzed using the DAVID tool for gene ontology (GO) biological processes (56,57). For differentially expressed lncRNAs, gene symbols including 'LINC' or '-AS1' were selected. Shared lncRNAs of SETD6 and TWIST1 were identified using venn diagram (http://bioinformatics.psb.ugent.be/webtools/Venn/).

Downloaded from https://academic.oup.com/nar/advance-article/doi/10.1093/nar/gkac485/6606173 by Ben Gurion University of the Negev-Medical Library user on 15 June 2022

LINC-PINT gene region was analyzed using the UCSC genome browser for promoter region (H3K4me3), regulatory elements (H3K27Ac) and TF clusters. 210 common target genes for SETD6 and TWIST1 were analyzed in the Enrichr database for ENCODE TF ChIP-seq and Epigenomics Roadmap HM ChIP-seq. 33 common target genes of SETD6, TWIST1 and LINC-PINT were analyzed using the DAVID tool for GO biological processes.

Statistical analyses

Statistical analyses for all assays were performed with GraphPad Prism software, using one-way or two-way analysis of variance (ANOVA) with a Tukey's post hoc test.

RESULTS

SETD6 levels increase in glioma and correlate with poor prognosis and EMT

We utilized the GlioVis bioinformatic tool (http://gliovis.bioinfo.cnio.es/) to study SETD6 levels in glioma patients. SETD6 mRNA levels are significantly increased in glioma patients in general ($n = 385$), and in the specific histological subtypes, oligodendroglioma ($n = 67$), astrocytoma ($n = 147$) and GBM ($n = 219$), compared to non-tumor samples ($n = 28$) (Figure 1A and B). Complementary to these findings, Kaplan–Meier survival analysis of glioma patients, taken from the CGGA ($n = 633$), and the Rembrandt ($n = 397$) datasets, revealed that SETD6 might serve as a predictor for overall survival. Patients with high expression of SETD6 had a significantly lower survival rate than patients with low expression (Figure 1C and D). A similar trend was observed in the TCGA database, albeit not statistically significant (Figure 1E). These findings suggest that SETD6 might promote oncogenic processes in glioma.

To study the potential role of SETD6 in glioma, we next performed an RNA-seq experiment using U251 control (CT) and two SETD6 CRISPR knock-out (KO) cells derived from two independent gRNAs clones (Figure 1F). Sequence validation of the two KO cells is shown in Supplementary Figure S1A. In this analysis, 2104 differentially expressed genes were identified (P-adj < 0.05); of these, 1190 genes were down-regulated and 914 were up-regulated in the CRISPR SETD6 KO cells (Figure 1F). Gene set enrichment analysis (GSEA) of hallmark gene sets revealed a significant enrichment of EMT in the down-regulated genes which is known to be a key regulatory process in glioma (58–60) (Figure 1G and H). For the up-regulated genes, we observed less significant results, with an enrichment of pathways linked to inflammation and oncogenic processes (Supplementary Figure S1B and C), processes in which we and others have shown the involvement of SETD6 (31,61). EMT is known to contribute to the aggressive phenotype of glioma (62–65). We then hypothesize that SETD6 might promote glioma through the regulation of EMT. The transcription factors SLUG, SNAIL, TWIST1 and ZEB1 are major regulators of the EMT process in glioma (16,66). To further support our hypothesis, we have performed a gene correlation analysis of SETD6 mRNA levels and the EMT-related transcription factors SNAIL, SLUG, ZEB1 and TWIST1 in glioma patients (Figure 1I–L). We used the CGGA database since it showed the strongest correlation between SETD6 levels and survival rates. The analysis revealed a positive correlation with all these genes, suggesting that SETD6 might promote EMT in glioma.

SETD6 binds and methylates TWIST1 in-vitro and in cells

Next, we hypothesized that SETD6 may have a functional link to one or more of these factors. To this end, we first expressed and purified the recombinant proteins SLUG, SNAIL and TWIST1. For technical reasons, we were unable to purify ZEB1 (data not shown). We first assessed the potential direct interactions between SETD6 and these proteins using ELISA. A direct interaction was observed between SETD6 and TWIST1, no interaction was observed between SETD6 and SNAIL, and a moderate but significant interaction was seen with SLUG. GST and BSA served as negative controls for these experiments (Figure 2A). To further analyze the interaction of SETD6 and TWIST1 in cells, we co-transfected HA-SETD6 and FLAG-TWIST1 in HEK293T cells followed by immunoprecipitation. As shown in Figure 2B, SETD6 interacts with immunoprecipitated TWIST1. Since TWIST1 is a transcription factor and localized primarily to the nucleus (67) and due to the established role of SETD6 in transcription regulation (33,36), we hypothesized that the interaction takes place on chromatin. Co-immunoprecipitation experiments within an isolated chromatin fraction in SETD6-KO HEK293T cells confirmed that the two proteins interact at chromatin (Figure 2C).

Given the enzymatic activity of SETD6 (68,69) and its physical interaction with TWIST1 *in-vitro* and in cells, we hypothesized that SETD6 methylates TWIST1. In an *in-vitro* methylation assay containing recombinant His-TWIST1, GST-SETD6 and tritium labeled SAM (*S*-adenosyl-methionine, the methyl donor), we found that SETD6 methylates TWIST1 and not the negative control BSA (Figure 2D). We could not detect any methylation of SNAIL. Furthermore, a weak methylation signal was detected for SLUG (Supplementary Figure S2) which is consistent with the results shown in Figure 2A. To validate whether SETD6 methylates TWIST1 in cells, we extracted the chromatin fraction of U251 SETD6 KO cells overexpressing exogenous FLAG-TWIST, with or without exogenous HA-SETD6 overexpression U251 cells, followed by immunoprecipitation with pan-methyl antibody. We found that the methylation of TWIST1 at chromatin in U251 cells was increased in the presence of SETD6 (Figure 2E). The weak signal in the absence of SETD6 (lane 2), suggests that TWIST1 is methylated by an additional methyltransferase. To further validate that SETD6 methylates TWIST1 at chromatin, we performed a reciprocal experiment in which FLAG-TWIST1 was immunoprecipitated from U251 chromatin extracts. As shown in Figure 2F, TWIST1 methylation increased in the presence of SETD6 overexpression. Taken together, our results show that SETD6 binds and methylates TWIST1 *in-vitro* and in cells at the chromatin.

Downloaded from https://academic.oup.com/nar/advance-article/doi/10.1093/nar/gkac485/6606173 by Ben Gurion University of the Negev-Medical Library user on 15 June 2022

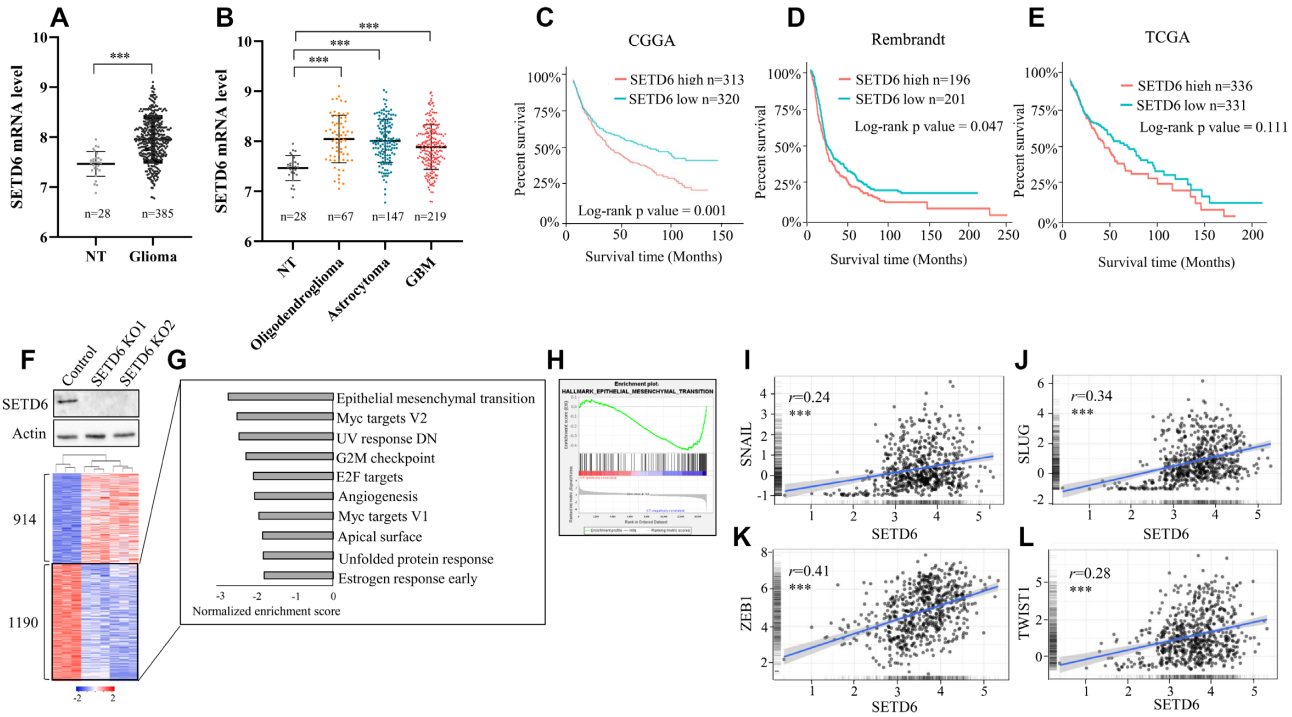

Figure 1. SETD6 levels increase in glioma and correlated with poor prognosis and EMT. (**A**) SETD6 mRNA levels of non-tumor (NT) ($n = 28$) and glioma patient samples ($n = 385$) are presented. (**B**) Glioma samples were divided according to their histological subtypes and SETD6 mRNA levels were extracted. The data was generated using the REMBRANDT dataset. *** $P < 0.001$. Kaplan–Meier survival curve of glioma patients stratified by high and low SETD6 expression levels from the CGGA (**C**), the REMBRANDT (**D**) and the TCGA (**E**) datasets. All graphs were generated using the GlioVis data portal. (**F**) U251 control and CRISPR SETD6 KO cells (two independent gRNAs) were subjected to western blot analysis using SETD6 and Actin antibodies (Top). Bottom: Heatmap showing up- and down-regulated genes (P-value < 0.05) from RNA-seq analysis of the indicated cells. Red and blue colors represent high and low expression levels, respectively. (**G**) Differentially expressed genes were analyzed using the Gene set enrichment analysis (GSEA) platform. Hallmark gene sets enriched in genes downregulated in SETD6 KO cells are presented according to their normalized enrichment score. (**H**) Enrichment plot of EMT gene set extracted from the GSEA analysis. The y-axis shows the enrichment score for each gene in the gene set (vertical black line represents each gene). Red (high) and blue (low) represent the expression levels in SETD6 KO cells versus control cells. Gene correlation analysis of SETD6 and SNAIL (**I**), SLUG (**J**), ZEB1 (**K**) and TWIST1 (**L**) using the CGGA dataset of glioma patients. Pearson's correlation coefficient (r) and statistical significance are presented *** P-value < 0.001. The data was extracted from the GlioVis data portal.

TWIST1 function in cell-ECM adhesion and migration is SETD6 dependent

Given the transcriptional activity mediated by SETD6 in U251 shown in Figure 1C and the methylation of TWIST1 by SETD6, we hypothesized that both proteins participate in the regulation of similar transcriptional programs. To address this, we have performed RNA-seq experiment in U251 cells stably expressing FLAG-TWIST1 (Figure 3A) and then compared the data with the differentially expressed genes regulated by SETD6. A total of 1075 genes were differentially expressed ($P < 0.05$) between FLAG-TWIST1 to empty vector expressing cells. As expected, EMT and extracellular matrix related-processes were highly enriched in FLAG-TWIST1 expressing cells (Supplementary Figure S3A and B). Among the 1075 genes, 210 SETD6 and TWIST1 shared genes were identified (P-value < $1.6E^{-19}$) (Figure 3B). In a gene ontology (GO) analysis, we identified significant enrichment of processes related to EMT such as ECM organization, collagen organization, cell adhesion and migration (Figure 3C). We therefore asked if TWIST1 expression regulates these processes in a SETD6-dependent manner. In a cell adhesion assay performed on Fibronectin and Collagen I (ECM proteins) coated wells, we observed loss of cell adhesion in cells stably expressing TWIST1. However, when TWIST1 was expressed in SETD6-depleted cells, we observed a similar level of cell-ECM adhesion as the control cells (Figure 3D and E). Western blots for the different cells used in these experiments are shown in Supplementary Figure S3C. Similar results were observed in a cell adhesion assay without adding any external ECM protein, counting on the ECM molecules secreted by the cells (Supplementary Figure S3D). Next, we tested the migration abilities of the cells in a wound-healing assay (Figure 3F). Consistent with previous studies (70,71), control cells stably expressing TWIST1 migrated faster than control cells expressing the empty vector. However, cells stably expressing TWIST1 in the absence of SETD6 had significantly lower migration abilities. SETD6-KO cells expressing empty vector showed a slight decrease in the migration abilities compared to control cells. This observation suggests that SETD6 affects migration in other mechanisms. Together, our results indicate that TWIST1 induction of loss of cell-ECM adhesion and increased migration are SETD6-dependent.

Downloaded from https://academic.oup.com/nar/advance-article/doi/10.1093/nar/gkac485/6606173 by Ben Gurion University of the Negev-Medical Library user on 15 June 2022

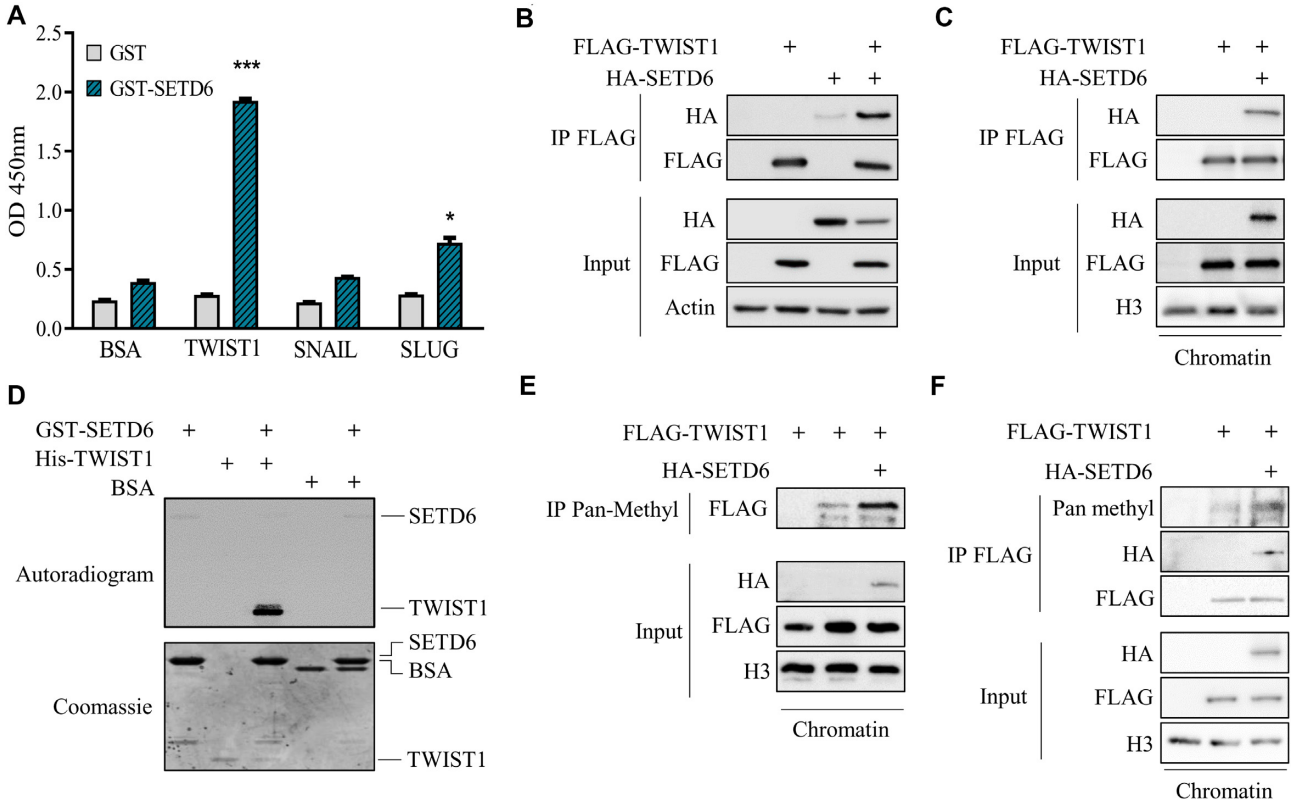

Figure 2. SETD6 interacts and methylates TWIST1 *in vitro* and in cells. (**A**) Enzyme-linked immunosorbent assay (ELISA) was performed with the indicated recombinant proteins. The graph represents absorbance at 450nm for each condition. (B, C) Human embryonic kidney (HEK) 293T cells were transfected with FLAG-TWIST1 with or without HA-SETD6. Whole cell lysates (**B**) or chromatin fraction (**C**) were immunoprecipitated with FLAG-M2 beads, followed by Western blot analysis with indicated antibodies. (**D**) *In vitro* methylation of TWIST1 by SETD6. Samples were subjected to SDS–polyacrylamide gel electrophoresis (PAGE) followed by exposure to autoradiogram to detect ^{3}H-labeled proteins or Coomassie staining to detect all proteins. BSA used as a negative control. (E, F) SETD6 KO U251 cells were transfected with FLAG-TWIST1 with or without HA-SETD6. Chromatin fractions were immunoprecipitated with Pan-Methyl lysine antibody (**E**) or FLAG-M2 beads (**F**), followed by Western blot analysis with the indicated antibodies.

SETD6 methylates TWIST1 on lysine 33

In order to map the methylation site, we performed non-radioactive methylation assay followed by mass spectrometry analysis. Among the 10 lysine residues found in TWIST1, lysine-33 and lysine-73 were identified as methylated by the mass spectrometry analysis (Figure 4A and B). However, the K73 methylation was also detected in the sample with no SAM (negative control). Both residues are within glycine-lysine motifs that were shown before to potentially serve as good predictor for methylation by SETD6 (72). For validation, we have generated methylation-deficient TWIST1 mutants at lysine-33 and lysine-73 to arginine (K33R, K73R) using site-directed mutagenesis. Sequence validation for the mutagenesis is shown in Supplementary Figure S4. In a radioactive methylation assay in the presence of GST-SETD6 with either WT TWIST1 or K33R, K73R mutants, we observed a decrease in the methylation signal for K33R mutant but not for K73R mutant (Figure 4C). In addition, we found that immunoprecipitated K33R TWIST1 from chromatin fraction of HEK293T cells is less methylated *in-vitro* by recombinant SETD6 compared to WT TWIST1 (Figure 4D). We next generated a site-specific antibody for TWIST1 K33me which specifically recognized a TWIST1 mono-methylated peptide at K33 but not the unmodified one (Figure 4E). Using this antibody, we could confirm the methylation of stable over-expressed TWIST1 WT in U251 but not TWIST1 harboring a K33R mutation (Figure 4F). To validate that TWIST1 K33me1 is SETD6 dependent, we immunoprecipitated FLAG-TWIST1 WT from HEK293T and U251 control and SETD6 KO cells (Figures 4G and H, respectively). A significant decrease in TWIST1 methylation was observed in the KOs of both cell lines. Taken together, these results suggest that lysine 33 is the primary methylation site by SETD6 *in vitro* and in cells.

Methylated TWIST1 is enriched at the long non-coding RNA LINC-PINT locus

Our RNA-seq data revealed that both SETD6 and TWIST1 regulate the expression of several long non-coding RNAs (LncRNAs) (Figure 5A). Among the 28 common LncRNAs, 8 had a fold change of >1.5 (Figure 5B). We hypothesized that SETD6-dependent TWIST1 methylation might regulate the expression of these lncRNAs. We have decided to focus on LINC-PINT since previous studies connected its expression with inhibition of cell migration and invasion in several cancer types, including glioma (39,40,73,74).

Downloaded from https://academic.oup.com/nar/advance-article/doi/10.1093/nar/gkac485/6606173 by Ben Gurion University of the Negev-Medical Library user on 15 June 2022

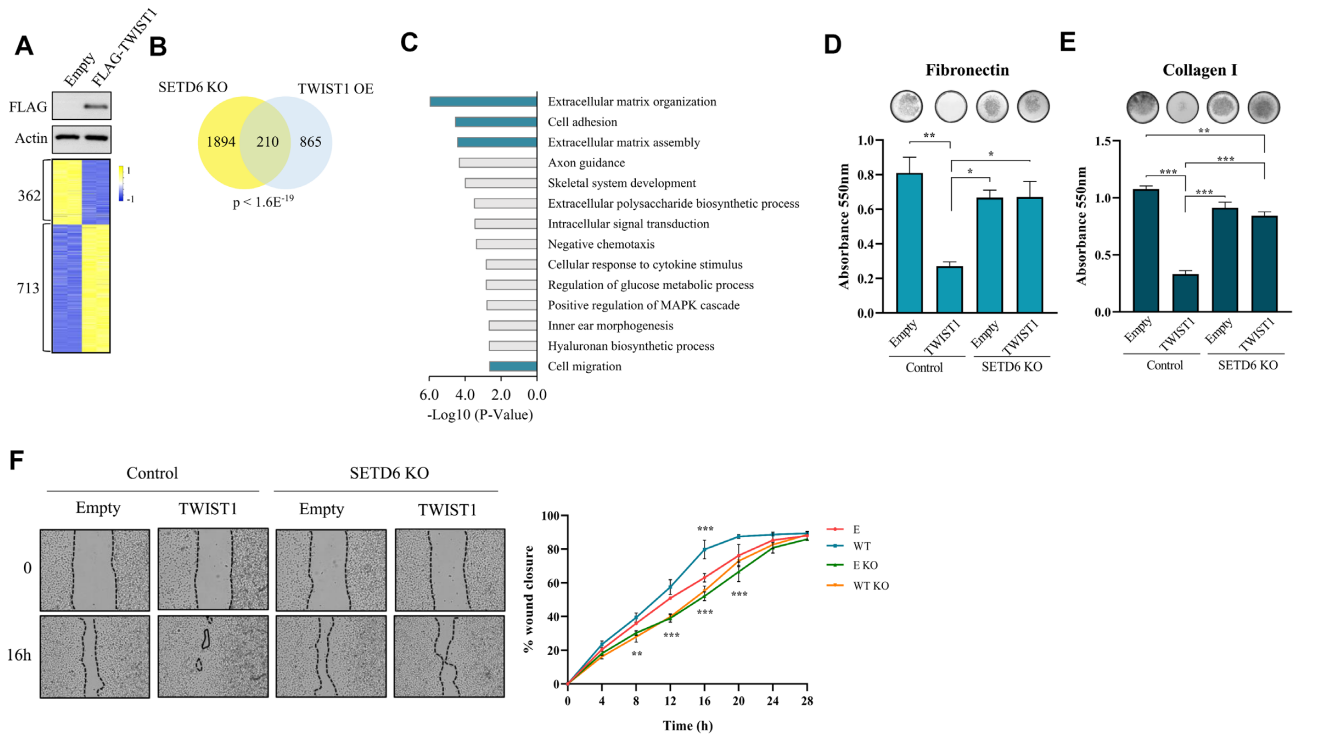

Figure 3. TWIST1 function in cell-ECM adhesion and migration is SETD6 dependent (**A**) U251 stably expressing empty vector or FLAG-TWIST1 were subjected to Western blot analysis with the indicated antibodies (top). Heatmap showing up-and down-regulated genes (P-value < 0.05) from RNA-seq analysis of the indicated cells. color bar represents high (yellow) and low (blue) expression levels. (**B**) Venn diagram showing common genes for TWIST1 and SETD6 as identified in the RNA-seq analyses. (**C**) Common genes were analyzed using the DAVID database. The most significantly enriched biological processes are presented (P-value < 0.05) and relevant processes are highlighted in cyan. (**D**) Fibronectin and Collagen I (**E**) adhesion assay with the indicated cells. Top: representative images of adherent cells stained with Crystal violet. Bottom: Crystal violet-stained cells were dissolved in 2% SDS and the absorbance at 550nm was measured. (**F**) Wound healing assay with the indicated cells. Confluent cells were scratched with 200ul pipette tip. Wound closure was monitored and calculated by Lionheart™ FX automated microscope and representative images at 0 and 16 h are shown with black lines indicating wound edges (left). Right: % wound closure (mean + SEM) of each cell type is shown. Statistical significance of each time point was calculated using two-way ANOVA (*P < 0.05, ** P < 0.01, *** P < 0.001). Asterisks on top represents statistical significance of FLAG-TWIST versus empty vector expressing cells. Asterisks on the bottom represents statistical significance of FLAG-TWIST1 vs. FLAG-TWIST1 SETD6 KO expressing cells.

By exploring the genomic location of LINC-PINT on chromosome 7q32.3, we have identified two potential TWIST1 binding sites (BS1 and BS2) by searching for E-box elements (Figure 5C). Using chromatin immunoprecipitation (ChIP) experiments, we revealed enrichment of endogenous TWIST1 on BS1 and BS2, confirming the hypothesis that TWIST1 binds the LINC-PINT locus in these locations (Figure 5D). In contrast, the occupancy of endogenous TWIST1 was significantly reduced in SETD6 KO cells at both binding sites, suggesting that TWIST1 occupancy is SETD6 dependent (Figure 5D). Consistent with these findings, the occupancy of FLAG-TWIST1 WT was significantly higher compared to Flag-TWIST1 K33R mutant at BS1 and BS2 regions (Figure 5E), indicating that the presence of TWIST1 on LINC-PINT locus is dependent on K33 methylation.

TWIST1 methylation negatively regulates the expression of LINC-PINT

Based on the observations that LINC-PINT expression is augmented and TWIST occupancy at the LINC-PINT locus is reduced under conditions of either TWIST-K33R expression or SETD6 KO, our working hypothesis was that this methylation event regulates the expression of LINC-PINT. To address this hypothesis, we first tested by qPCR the expression of LINC-PINT and found a significant increase under conditions of SETD6 KO compared to control cells (Figure 6A). Consistent with these results, an increase in LINC-PINT levels was seen in cells stably expressing TWIST1 K33R mutant compared to TWIST1 WT (Figure 6B). Together, our results suggest that methylated TWIST1 binds the LINC-PINT locus and inhibits its expression in a SETD6 and a methylation dependent manner.

We next sought for the mechanism by which TWIST1 methylation inhibits LINC-PINT expression. To address this, we analyzed TWIST1 and SETD6 common target genes using the Enrichr platform (75–77) for ENCODE TF (http://genome.ucsc.edu/ENCODE/downloads.html) (Figure 6C) and Epigenomics Roadmap (http://www.roadmapepigenomics.org/data) (Figure 6D) ChIP-seq databases. Both platforms integrate a large collection of ChIP-seq data to predict protein interaction with the DNA (44,78). The results demonstrate a significant enrichment of the PRC2 (Polycomb repressive complex 2) components EZH2 and SUZ12 (Figure 6C) and a significant enrichment for H3K27me3 (Figure 6D), a chromatin repressive mark catalyzed by EZH2 (79), associated with gene silenc-

Downloaded from https://academic.oup.com/nar/advance-article/doi/10.1093/nar/gkac485/6606173 by Ben Gurion University of the Negev-Medical Library user on 15 June 2022

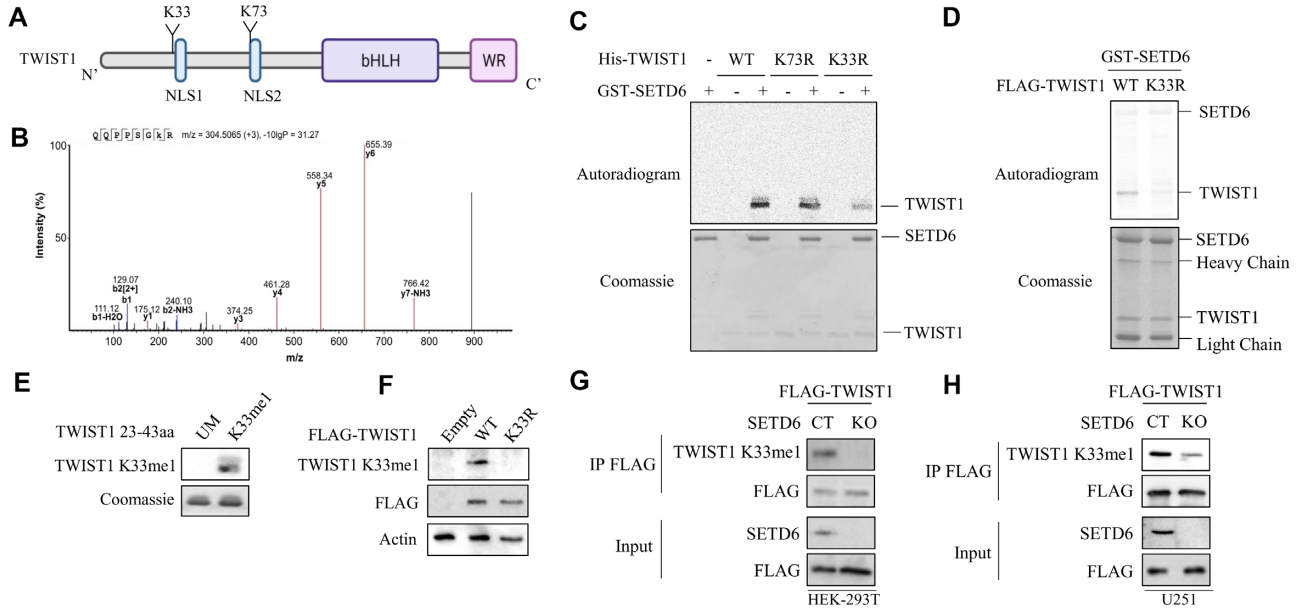

Figure 4. SETD6 methylates TWIST1 at K33. (**A**) Illustration of TWIST1 sequence and domains with the identified methylated lysine residues (NLS-nuclear localization sequence, bHLH-basic-helix-loop-helix). (**B**) In vitro methylation assay was performed with recombinant His-TWIST1 and GST-SETD6 with or without SAM followed by mass spectrometry analysis. MS spectra of TWIST1 QQPPSGKR peptide is shown. The MS spectra was visualized with PEAKS software. Major y- and b-ions are displayed as red, and blue, respectively. The m/z ratio of labelled ions are shown above each ion label. Mono-methylated lysine is indicated as a lowercase 'k'. For the parent ion, mass-to-charge ratio (m/z), overall charge, and PEAKS score (-10lgP) are shown above the spectrum. (**C**) MS results were validated by *in vitro* methylation assay with the indicated recombinant proteins in the presence of ^{3}H-labeled SAM. (**D**) semi-*in vitro* methylation assay. HEK293T SETD6 KO cells were transfected with FLAG-TWIST1 WT or K33R mutant. Chromatin fractions were immunoprecipitated with FLAG-M2 beads and were subjected to radioactive *in vitro* methylation assay with recombinant SETD6. Autoradiogram used to detect ^{3}H-labeled proteins and Coomassie staining to detect all proteins. (**E**) TWIST1 peptides (Unmodified and K33me1) were subjected to SDS-PAGE followed by western blot analysis with K33me1 antibody and coomassie staining. (**F**) Western blot analysis of U251 stably expressing empty vector, FLAG-TWIST1 WT or K33R cells with the indicated antibodies. (**G**) HEK293T or U251 (H) control and SETD6 KO cells were transfected with FLAG-TWIST1 and immunoprecipitated with FLAG-M2 beads followed by Western blot analysis with the indicated antibodies.

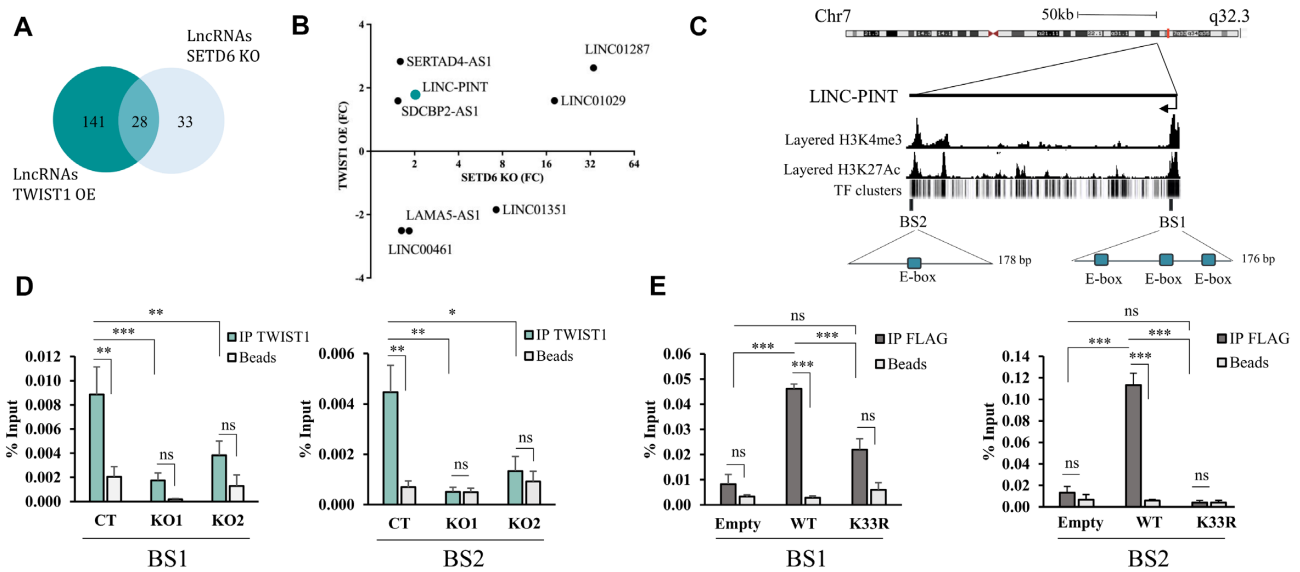

Figure 5. Methylated TWIST1 binds LINC-PINT gene region. (**A**) Venn diagram showing lncRNAs regulated by both SETD6 and TWIST1, which identified in the previous RNA-seq experiments. (**B**) Graph of top 8 shared lncRNAs (FC > 1.5) with their FC in SETD6 KO cells (x-axis) and cells stably express FLAG-TWIST1 (y-axis). (**C**) LINC-PINT genomic region. Layered H3K4me3, H3K27Ac and TF clusters were extracted from the UCSC genome browser. The two TWIST1 binding sites (BS1 and BS2) used for ChIP assays are shown. E-boxes inside each binding site are indicated. (**D**) ChIP assays of U251 SETD6 KO cells immunoprecipitated with TWIST1 antibody or beads as negative control. (**E**) ChIP assay of U251 stably expressing empty vector, FLAG-TWIST1 WT or K33R cells immunoprecipitated with FLAG-M2 beads. (D, E) Graphs show % input of the quantified DNA. Error bars are SEM. Statistical significance was calculated using two-way ANOVA for three experimental repeats (ns, non-significant, * $P < 0.05$, ** $P < 0.01$, *** $P < 0.001$).

Downloaded from https://academic.oup.com/nar/advance-article/doi/10.1093/nar/gkac485/6606173 by Ben Gurion University of the Negev-Medical Library user on 15 June 2022

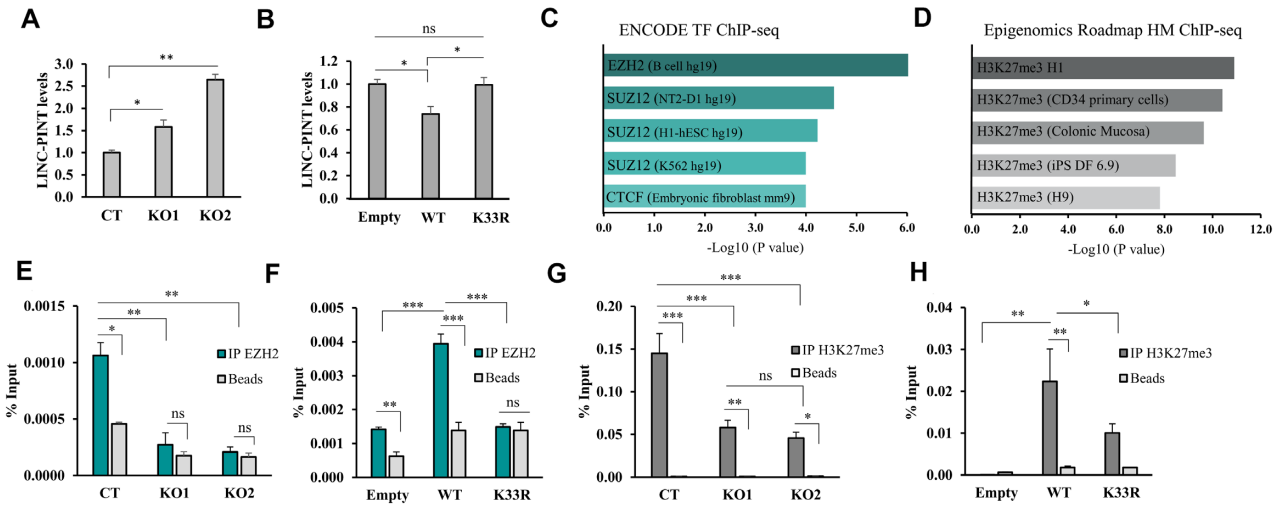

Figure 6. Methylated TWIST1 inhibit LINC-PINT expression. (**A**) RNA was extracted from U251 SETD6 KO or U251 stably expressing empty vector, FLAG-TWIST1 WT or K33R cells (**B**) and expression level were measured by quantitative polymerase chain reaction (qPCR). mRNA levels were normalized to glyceraldehyde-3-phosphate dehydrogenase (GAPDH) and then to empty cells. Error bars are SEM. Statistical analysis was performed for three experimental repeats using one-way ANOVA (*$P < 0.05$, **$P < 0.01$). (C, D) Common target genes of TWIST1 and SETD6 were analyzed by the Enrichr platform. Top 5 Transcription factors from ENCODE TF ChIP-seq (**C**) and Histone marks from the Epigenomics Roadmap HM ChIP-seq (**D**) are presented with the cell line and genome used in the ChIP-seq experiments. (**E-H**) ChIP assays. Chromatin fractions of the indicated cell type were immunoprecipitated with EZH2 (E, F) or H3K27me3 (G + H) antibodies or beads as negative control, followed by qPCR of LINC-PINT locus. Graphs show % input of the quantified DNA. Error bars are SEM. Statistical significance was calculated using two-way ANOVA for three experimental repeats (ns, non-significant, * $P < 0.05$, **$P < 0.01$, ***$P < 0.001$).

ing (80). A snapshot of ChIP-seq data showing the enrichment of EZH2 and H3K27me3 in a brain tissue at this genomic location is shown in Supplementary Figure S5A. To validate these results, we performed ChIP experiments to test the occupancy of EZH2 and H3K27me3 on the LINC-PINT locus. As shown in Figure 6E, the enrichment of the methyltransferase EZH2 decreased in the SETD6 KO cells at the LINC-PINT locus. As predicted and consistent with our working model, EZH2 displayed significantly higher enrichment in cell expressing TWIST1 WT compared to TWIST1 K33R mutant (Figure 6F). Likewise, H3K27me3 was significantly lower in the SETD6 KO and cells stably expressing TWIST1 K33R, two conditions which represent un-methylated status of TWIST1 at K33 (Figure 6G and H, respectively). We further confirmed that the decrease in the occupancy of H3K27me3 is not due to a decrease in total H3 (Supplementary Figures S5B, C). To validate the specificity of the antibodies used for ChIP experiments, we compared the enrichment of EZH2, H3K27me3 and H3 on LINC-PINT locus with general mouse IgG (Supplementary Figure S5D). Taken together, these results suggest that TWIST1 methylation at K33 by SETD6 represses LINC-PINT transcription by increasing the occupancy of EZH2 and the catalysis of H3K27me3 repressive mark.

TWIST1 mediated-inhibition of LINC-PINT leads to loss of cell adhesion and increased migration

Integration of our RNA-seq data of SETD6 (Figure 1F) and TWIST1 (Figure 3A) target genes with previously published LINC-PINT target genes (38), revealed 33 common target genes (Figure 7A). GO analysis for biological processes found enrichment of extracellular matrix organization (Figure 7A and B). LINC-PINT was shown before to regulate cell adhesion genes and to inhibit migration of cancer cells (39,81). We therefore hypothesized that cells expressing un-methylated TWIST1 (K33R mutant), which induces the expression of LINC-PINT RNA, will display similar phenotypes to cells expressing LINC-PINT. To address this hypothesis, we have generated cells stably expressing TWIST1 WT, K33R mutant and LINC-PINT and tested adhesion and migration abilities (Figure 7C, and Supplementary Figure S6A and B for expression validation). Consistent with the results obtained in Figure 3D, we found reduced adhesion in cells expressing TWIST1 WT. However, a significant increase in cell adhesion was observed in cells expressing TWIST1 K33R and LINC-PINT (Figure 7C). A significant inhibition in the ability of cells to close the wound in a wound-healing assay was observed in cells stably expressing TWIST1 K33R and LINC-PINT compared to TWIST1 WT (Figure 7D). To test whether the methylation and not the interaction with SETD6 is responsible for the observed phenotypes, we tested the effect of K33R mutation on TWIST1-SETD6 interaction using ELISA and Co-Immunoprecipitation experiments. In the ELISA assay, K33R mutation did not reduced the interaction with GST-SETD6. Similar results were observed in immunoprecipitated FLAG-TWIST1 from HEK293T in the presence of HA-SETD6 (Supplementary Figure S6C and D). Thus, we concluded that K33 methylation and not the physical interaction with SETD6 is responsible for the observed phenotypes. In summary, our findings demonstrate that SETD6 selectively regulates the expression of LINC-PINT RNA. SETD6-mediated methylation of TWIST1 at K33 represses the expression of LINC-PINT by increasing H3K27me3 repressive mark at the LINC-PINT locus. Under permissive conditions, when TWIST1 is not methylated (SETD6-depletion or expression of TWIST1 K33R

Downloaded from https://academic.oup.com/nar/advance-article/doi/10.1093/nar/gkac485/6606173 by Ben Gurion University of the Negev-Medical Library user on 15 June 2022

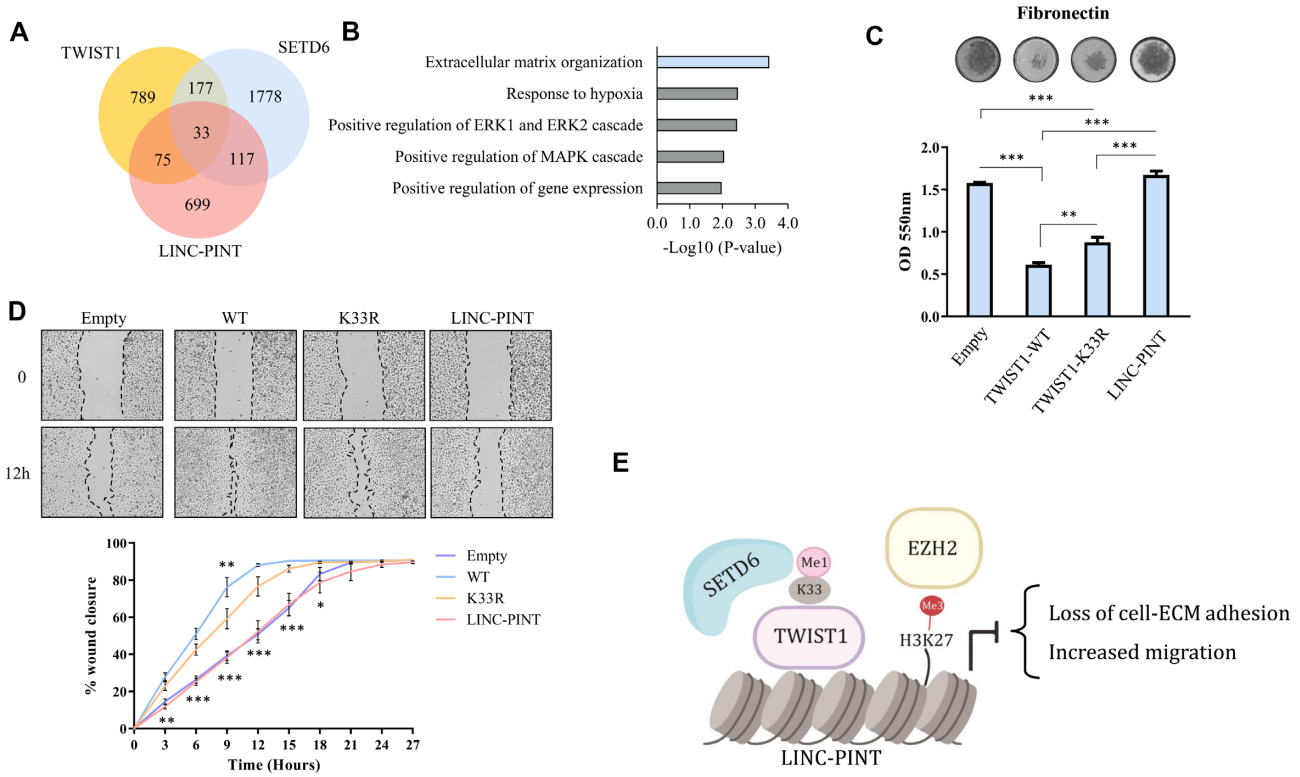

Figure 7. TWIST1 mediated-inhibition of LINC-PINT leads to loss of cell adhesion and increased migration. (**A**) Venn diagram showing common target genes for SETD6, TWIST1 and LINC-PINT. LINC-PINT target genes were taken from LINC-PINT KD HCT116 cells (38). (**B**) 33 common genes were analyzed using the DAVID database. Top 5 Significantly enriched biological processes are presented. Biological process of interest is highlighted in light blue. (**C**) Fibronectin adhesion assay with the indicated cells. Top: representative images of fibronectin-adherent cells stained with Crystal violet. Bottom: Crystal violet-stained cells were dissolved and the absorbance at 550 nm was measured. (**D**) Wound healing assay with the indicated cells. Confluent cells were scratched with 200 ul pipette tip. Wound closure was monitored and calculated by Lionheart™ FX automated microscope and representative images at 0 and 12 h are shown with black lines indicating wound edges (top). Bottom: % wound closure (mean + SEM) of each time point and cell type is shown. Statistical significance was calculated using two-way ANOVA for cells stably expressing TWIST1 WT versus LINC-PINT (below the graph) and for TWIST1 WT versus K33R (above the graph) (*$P < 0.05$, ** $P < 0.01$, *** $P < 0.001$). (**E**) Schematic model illustrating the inhibition of LINC-PINT expression by TWIST1 methylation. Following TWIST1 K33 methylation by SETD6, EZH2 is recruited to LINC-PINT locus and inhibits its expression through the induction of H3K27 tri-methylation. LINC-PINT inhibition leads loss of cell-ECM adhesion and increased migration.

mutant), TWIST1 dissociates from the LINC PINT locus, H3K27me3 mark is decreased allowing the increase in LINC-PINT expression level to increase cell adhesion and to reduce cell migration (Figure 7E).

DISCUSSION

Bioinformatic analysis for SETD6 expression in glioma patients and U251 glioma-derived cells revealed two interesting observations; First, SETD6 levels increase in all glioma subtypes and correlated with poor prognosis. Second, gene correlation analysis of SETD6 expression levels from these patients and from our RNA-seq experiments have suggested that SETD6 promotes EMT. Based on these observations we hypothesized that SETD6 may regulate glioma through a functional crosstalk with one of the key cellular EMT-related transcription factors: SNAIL, SLUG, TWIST1 and ZEB. While all these transcription factors were shown to play key role in glioma (13–17), TWIST1 showed the most compelling results with regards to SETD6.

In recent years, the biology of LINC-PINT has been studied in several cancer models, including glioma, and was shown to be activated by p53 in some of them (38,39). Thus, it is not surprising that similarly to p53, its expression is downregulated in various cancers and exhibits tumor suppressor cellular properties like inhibition of proliferation, migration and invasion (39,73,74,81). Beside the several p53 binding sites along the LINC-PINT genomic locus that were characterized by others (38), here we propose that LINC-PINT expression is also transcriptionally modulated by TWIST1, and its expression is selectively regulated by the methylation status of TWIST1. This selective activation, mediated by SETD6, allows fine tuning of LINC-PINT expression and biological functions.

How the methylation of TWIST1 directly regulates the expression of LINC-PINT remains an open question. Here we provide molecular evidence that TWIST1 methylation by SETD6 at K33 increases the occupancy of EZH2 and the H3K27me3 repressive mark at the LINC-PINT locus. However, we still do not fully understand the molecular link between TWIST1 and EZH2 recruitment to the LINC-PINT locus. Interestingly, TWIST1 was shown to recruit EZH2 to repress the expression of its target genes by increasing the H3K27me3 mark at their promotors (82). A similar mechanism might exist at the LINC-PINT locus; however this hypothesis requires further investigation.

Downloaded from https://academic.oup.com/nar/advance-article/doi/10.1093/nar/gkac485/6606173 by Ben Gurion University of the Negev-Medical Library user on 15 June 2022

Similar to previous observations that LINC-PINT repression of downstream target genes is mediated by H3K27me3 (38,39), our data suggest that LINC-PINT own transcription regulation might be controlled by the same protein complex, in a TWIST1 methylation dependent manner. However, TWIST1 methylation can affect transcription via several mechanisms. For example, the methylation can modulate TWIST1 interaction with its homo/heterodimer natural partners (83,84). In addition, the methylation can directly determine TWIST1 affinity to the DNA as was shown for other transcription factors such as p53, YY1 and NF-kappaB (85–87).

An intriguing possibility, that potentially has to be validated is that LINC-PINT regulates its own expression in a positive feedback loop mechanism. While this closed chromatin state can partially explain why LINC-PINT expression is repressed in the presence of SETD6, future biochemical and structural characterizations are required to address several remaining open questions. For example: How does TWIST1 methylation recruits these factors? What is the kinetic of this phenomenon? What are the protein complexes that are recruited to the LINC-PINT locus and why does the lack of TWIST1-K33 methylation enable the increased expression of LINC-PINT?

As described in detail in the introduction, TWIST1 is subjected to numerous post-translational modifications (24–29). However, to the best of our knowledge this is the first report which shows that it is subjected to lysine methylation. Our data suggests that TWIST1 might be also methylated on additional lysine residues in a SETD6-dependent and independent manner. Future experiments will determine the contribution of additional methylation sites to TWIST1 cellular activity which are probably mediated by other methyl-transferases. The cross-talk between these modifications will shed new light on its cellular activities.

We have investigated the effect of TWIST1 methylation on cell-ECM adhesion and migration in two cellular setups: (i) cells stably expressing TWIST1 in the absence of SETD6; and (ii) cells stably expressing TWIST1 K33R. We expected similar phenotypes in both setups, as both reflect an un-methylated state of TWIST1. However, cells stably expressing TWIST1 K33R showed milder effects compared to TWIST1 WT in SETD6-depleted cells. One explanation could be that in addition to K33 there is another methylated residue, which is still methylated and functional in cells expressing TWIST1 K33R. Another possible explanation might be that SETD6 affects cell adhesion and migration through another TWIST1-independant mechanism (as recently published (88)).

Our data supports a model by which the methylation of TWIST1 at K33 by SETD6 reduces cell-ECM adhesion while increasing cellular migration. These results are consistent with the classic view, that during malignant transformation and specifically during EMT, cells lose their cell-cell and cell-ECM interactions, allowing them increased motile and invasive properties (12,89). On the other hand, binding to the ECM was shown before to be crucial for generating cellular movement (90,91). With regards to TWIST1, Mikheeva *et al.* showed that in SNB19 GBM cells, TWIST1 over expression resulted in increased adhesion to fibronectin (17). Conversely, in hepatocellular carcinoma, TWIST1 over-expression reduced focal adhesions (92). Although these are opposing observations, both correlate with increased migration and invasion. The opposing reports regarding TWIST1 function in cell adhesion highlight the complexity of these two important phenotypes in cancer progression.

The correlation between SETD6 expression and the clinical outcome led us to investigate the role of this methyltransferase in glioma and enabled us to decipher a new avenue by which lysine methylation signaling controls TWIST1 activity at chromatin. Besides glioma, SETD6, TWIST1 and LINC-PINT are also expressed in several other cancers (93–95). We therefore speculate that the mechanism described in this paper can be expended and studied in other cancer models with the aim to translate these new findings for prognostic and therapeutic applications.

DATA AVAILABILITY

The RNA-seq data described in this study are deposited to the Gene Expression Omnibus (GEO) repository under accession number GSE186047.

All the Mass spectrometry data was submitted to the ProteomeXchange via the PRIDE database under Project accession number PXD029361.

SUPPLEMENTARY DATA

Supplementary Data are available at NAR Online.

ACKNOWLEDGEMENTS

We thank the Levy lab for technical assistance and helpful discussions. We thank Idan Cohen and Debbie Toiber for providing the EZH2 and H3K27me3 antibodies. We would also like to thank David Morgenstern for his help with the mass spectrometry data analysis.

Author contribution: L.E., M.F. and D.L. conceived and designed most of the experiments. A.C. and K.B. performed the mass spectrometry analysis. T.E. performed the experiments to validate the TWIST1K33me1 antibody. C.J.F. generated the TWIST1 K33me antibody. G.S. and N.S. performed the bioinformatic analysis. D.L., C.J.F., K.B., N.S. and M.T.B. helped with experimental design and provided valuable conceptual input for the study. L.E. and D.L. wrote the paper. All authors read and approved the final manuscript.

FUNDING

Israel Science Foundation [285/14, 262/18 to D.L.]; Israeli Cancer Research Foundation Israel (ICRF), from the Israel Cancer Association and from the BSF-NSF [BSF2019626/NSF1939814 to D.L., M.T.B.]. Funding for open access charge: Research Grants.

Conflict of interest statement. None declared.

REFERENCES

1. Rasmussen,B.K., Hansen,S., Laursen,R.J., Kosteljanetz,M., Schultz,H., Norgard,B.M., Guldberg,R. and Gradel,K.O. (2017)

Downloaded from https://academic.oup.com/nar/advance-article/doi/10.1093/nar/gkac485/6606173 by Ben Gurion University of the Negev-Medical Library user on 15 June 2022

Epidemiology of glioma: clinical characteristics, symptoms, and predictors of glioma patients grade I-IV in the the danish neuro-oncology registry. *J. Neurooncol.*, **135**, 571–579.
2. Ostrom,Q.T., Bauchet,L., Davis,F.G., Deltour,I., Fisher,J.L., Langer,C.E., Pekmezci,M., Schwartzbaum,J.A., Turner,M.C., Walsh,K.M. *et al.* (2014) The epidemiology of glioma in adults: a "state of the science" review. *Neuro-oncol.*, **16**, 896–913.
3. Ferlay,J., Colombet,M., Soerjomataram,I., Mathers,C., Parkin,D.M., Pineros,M., Znaor,A. and Bray,F. (2019) Estimating the global cancer incidence and mortality in 2018: GLOBOCAN sources and methods. *Int. J. Cancer*, **144**, 1941–1953.
4. Gore,S., Chougule,T., Jagtap,J., Saini,J. and Ingalhalikar,M. (2021) A review of radiomics and deep predictive modeling in glioma characterization. *Acad. Radiol.*, **28**, 1599–1621.
5. Tan,A.C., Ashley,D.M., Lopez,G.Y., Malinzak,M., Friedman,H.S. and Khasraw,M. (2020) Management of glioblastoma: state of the art and future directions. *CA Cancer J. Clin.*, **70**, 299–312.
6. Miller,K.D., Ostrom,Q.T., Kruchko,C., Patil,N., Tihan,T., Cioffi,G., Fuchs,H.E., Waite,K.A., Jemal,A., Siegel,R.L. *et al.* (2021) Brain and other central nervous system tumor statistics, 2021. *CA Cancer J. Clin.*, **71**, 381–406.
7. Zhang,J., Cai,H., Sun,L., Zhan,P., Chen,M., Zhang,F., Ran,Y. and Wan,J. (2018) LGR5, a novel functional glioma stem cell marker, promotes EMT by activating the Wnt/beta-catenin pathway and predicts poor survival of glioma patients. *J. Exp. Clin. Cancer Res.*, **37**, 225.
8. Theeler,B.J., Yung,W.K., Fuller,G.N. and De Groot,J.F. (2012) Moving toward molecular classification of diffuse gliomas in adults. *Neurology*, **79**, 1917–1926.
9. Reifenberger,G., Wirsching,H.G., Knobbe-Thomsen,C.B. and Weller,M. (2017) Advances in the molecular genetics of gliomas - implications for classification and therapy. *Nat. Rev. Clin. Oncol.*, **14**, 434–452.
10. Nieto,M.A., Huang,R.Y., Jackson,R.A. and Thiery,J.P. (2016) Emt: 2016. *Cell*, **166**, 21–45.
11. Thiery,J.P., Acloque,H., Huang,R.Y. and Nieto,M.A. (2009) Epithelial-mesenchymal transitions in development and disease. *Cell*, **139**, 871–890.
12. Kalluri,R. and Weinberg,R.A. (2009) The basics of epithelial-mesenchymal transition. *J. Clin. Invest.*, **119**, 1420–1428.
13. Lin,J.C., Tsai,J.T., Chao,T.Y., Ma,H.I. and Liu,W.H. (2018) The STAT3/Slug axis enhances radiation-induced tumor invasion and cancer Stem-like properties in radioresistant glioblastoma. *Cancers (Basel)*, **10**, 512.
14. Iwadate,Y. (2016) Epithelial-mesenchymal transition in glioblastoma progression. *Oncol. Lett.*, **11**, 1615–1620.
15. Siebzehnrubl,F.A., Silver,D.J., Tugertimur,B., Deleyrolle,L.P., Siebzehnrubl,D., Sarkisian,M.R., Devers,K.G., Yachnis,A.T., Kupper,M.D., Neal,D. *et al.* (2013) The ZEB1 pathway links glioblastoma initiation, invasion and chemoresistance. *EMBO Mol. Med.*, **5**, 1196–1212.
16. Han,S.P., Kim,J.H., Han,M.E., Sim,H.E., Kim,K.S., Yoon,S., Baek,S.Y., Kim,B.S. and Oh,S.O. (2011) SNAI1 is involved in the proliferation and migration of glioblastoma cells. *Cell. Mol. Neurobiol.*, **31**, 489–496.
17. Mikheeva,S.A., Mikheev,A.M., Petit,A., Beyer,R., Oxford,R.G., Khorasani,L., Maxwell,J.P., Glackin,C.A., Wakimoto,H., Gonzalez-Herrero,I. *et al.* (2010) TWIST1 promotes invasion through mesenchymal change in human glioblastoma. *Mol. Cancer*, **9**, 194.
18. Qin,Q., Xu,Y., He,T., Qin,C. and Xu,J. (2012) Normal and disease-related biological functions of twist1 and underlying molecular mechanisms. *Cell Res.*, **22**, 90–106.
19. Bouard,C., Terreux,R., Honorat,M., Manship,B., Ansieau,S., Vigneron,A.M., Puisieux,A. and Payen,L. (2016) Deciphering the molecular mechanisms underlying the binding of the TWIST1/E12 complex to regulatory E-box sequences. *Nucleic Acids Res.*, **44**, 5470–5489.
20. Connerney,J., Andreeva,V., Leshem,Y., Muentener,C., Mercado,M.A. and Spicer,D.B. (2006) Twist1 dimer selection regulates cranial suture patterning and fusion. *Dev. Dyn.*, **235**, 1345–1357.
21. Zhao,Z., Rahman,M.A., Chen,Z.G. and Shin,D.M. (2017) Multiple biological functions of twist1 in various cancers. *Oncotarget*, **8**, 20380–20393.
22. Zhu,Q.Q., Ma,C., Wang,Q., Song,Y. and Lv,T. (2016) The role of TWIST1 in epithelial-mesenchymal transition and cancers. *Tumour Biol.*, **37**, 185–197.
23. Velpula,K.K., Dasari,V.R., Tsung,A.J., Dinh,D.H. and Rao,J.S. (2011) Cord blood stem cells revert glioma stem cell EMT by down regulating transcriptional activation of sox2 and twist1. *Oncotarget*, **2**, 1028–1042.
24. Mikheeva,S.A., Camp,N.D., Huang,L., Jain,A., Jung,S.Y., Avci,N.G., Tokita,M., Wolf-Yadlin,A., Zhang,J., Tapscott,S.J. *et al.* (2019) TWIST1 heterodimerization with E12 requires coordinated protein phosphorylation to regulate periostin expression. *Cancers (Basel)*, **11**, 1392.
25. Hong,J., Zhou,J., Fu,J., He,T., Qin,J., Wang,L., Liao,L. and Xu,J. (2011) Phosphorylation of serine 68 of twist1 by MAPKs stabilizes twist1 protein and promotes breast cancer cell invasiveness. *Cancer Res.*, **71**, 3980–3990.
26. Ertosun,M.G., PehlIvanoGlu,S., S,D.I., TanriOver,G. and Oze,S.O. (2020) AKT-mediated phosphorylation of TWIST1 is essential for breast cancer cell metastasis. *Turk. J. Biol.*, **44**, 158–165.
27. Lee,H.J., Li,C.F., Ruan,D., Powers,S., Thompson,P.A., Frohman,M.A. and Chan,C.H. (2016) The DNA damage transducer RNF8 facilitates cancer chemoresistance and progression through twist activation. *Mol. Cell*, **63**, 1021–1033.
28. Avasarala,S., Van Scoyk,M., Karuppusamy Rathinam,M.K., Zerayesus,S., Zhao,X., Zhang,W., Pergande,M.R., Borgia,J.A., DeGregori,J., Port,J.D. *et al.* (2015) PRMT1 is a novel regulator of epithelial-mesenchymal-transition in Non-small cell lung cancer. *J. Biol. Chem.*, **290**, 13479–13489.
29. Shi,J., Wang,Y., Zeng,L., Wu,Y., Deng,J., Zhang,Q., Lin,Y., Li,J., Kang,T., Tao,M. *et al.* (2014) Disrupting the interaction of BRD4 with diacetylated twist suppresses tumorigenesis in basal-like breast cancer. *Cancer Cell*, **25**, 210–225.
30. Cornett,E.M., Ferry,L., Defossez,P.A. and Rothbart,S.B. (2019) Lysine methylation regulators moonlighting outside the epigenome. *Mol. Cell*, **75**, 1092–1101.
31. Levy,D., Kuo,A.J., Chang,Y., Schaefer,U., Kitson,C., Cheung,P., Espejo,A., Zee,B.M., Liu,C.L., Tangsombatvisit,S. *et al.* (2011) Lysine methylation of the NF-kappaB subunit RelA by SETD6 couples activity of the histone methyltransferase GLP at chromatin to tonic repression of NF-kappaB signaling. *Nat. Immunol.*, **12**, 29–36.
32. Feldman,M., Vershinin,Z., Goliand,I., Elia,N. and Levy,D. (2019) The methyltransferase SETD6 regulates mitotic progression through PLK1 methylation. *Proc. Natl. Acad. Sci. U.S.A.*, **116**, 1235–1240.
33. Vershinin,Z., Feldman,M., Chen,A. and Levy,D. (2016) PAK4 methylation by SETD6 promotes the activation of the Wnt/beta-Catenin pathway. *J. Biol. Chem.*, **291**, 6786–6795.
34. Chen,A., Feldman,M., Vershinin,Z. and Levy,D. (2016) SETD6 is a negative regulator of oxidative stress response. *Biochim. Biophys. Acta*, **1859**, 420–427.
35. O'Neill,D.J., Williamson,S.C., Alkharaif,D., Monteiro,I.C., Goudreault,M., Gaughan,L., Robson,C.N., Gingras,A.C. and Binda,O. (2014) SETD6 controls the expression of estrogen-responsive genes and proliferation of breast carcinoma cells. *Epigenetics*, **9**, 942–950.
36. Vershinin,Z., Feldman,M., Werner,T., Weil,L.E., Kublanovsky,M., Abaev-Schneiderman,E., Sklarz,M., Lam,E.Y.N., Alasad,K., Picaud,S. *et al.* (2021) BRD4 methylation by the methyltransferase SETD6 regulates selective transcription to control mRNA translation. *Sci. Adv.*, **7**, eabf5374.
37. Statello,L., Guo,C.J., Chen,L.L. and Huarte,M. (2021) Gene regulation by long non-coding RNAs and its biological functions. *Nat. Rev. Mol. Cell Biol.*, **22**, 96–118.
38. Marin-Bejar,O., Marchese,F.P., Athie,A., Sanchez,Y., Gonzalez,J., Segura,V., Huang,L., Moreno,I., Navarro,A., Monzo,M. *et al.* (2013) Pint lincRNA connects the p53 pathway with epigenetic silencing by the polycomb repressive complex 2. *Genome Biol.*, **14**, R104.
39. Marin-Bejar,O., Mas,A.M., Gonzalez,J., Martinez,D., Athie,A., Morales,X., Galduroz,M., Raimondi,I., Grossi,E., Guo,S. *et al.* (2017) The human lncRNA LINC-PINT inhibits tumor cell invasion through a highly conserved sequence element. *Genome Biol.*, **18**, 202.
40. Zhu,H., Chen,Z., Shen,L., Tang,T., Yang,M. and Zheng,X. (2020) Long noncoding RNA LINC-PINT suppresses cell proliferation, invasion, and EMT by blocking Wnt/beta-Catenin signaling in glioblastoma. *Front. Pharmacol.*, **11**, 586653.

Downloaded from https://academic.oup.com/nar/advance-article/doi/10.1093/nar/gkac485/6606173 by Ben Gurion University of the Negev-Medical Library user on 15 June 2022

41. Yang,X., Miao,S., Mao,X., Xiu,C., Sun,J., Pei,R. and Jia,S. (2021) LncRNA LINC-PINT inhibits malignant behaviors of laryngeal squamous cell carcinoma cells via inhibiting ZEB1. *Pathol. Oncol. Res.*, **27**, 584466.
42. Tzanakakis,G., Kavasi,R.M., Voudouri,K., Berdiaki,A., Spyridaki,I., Tsatsakis,A. and Nikitovic,D. (2018) Role of the extracellular matrix in cancer-associated epithelial to mesenchymal transition phenomenon. *Dev. Dyn.*, **247**, 368–381.
43. Encode Project Consortium (2012) An integrated encyclopedia of DNA elements in the human genome. *Nature*, **489**, 57–74.
44. Bernstein,B.E., Stamatoyannopoulos,J.A., Costello,J.F., Ren,B., Milosavljevic,A., Meissner,A., Kellis,M., Marra,M.A., Beaudet,A.L., Ecker,J.R. *et al.* (2010) The NIH roadmap epigenomics mapping consortium. *Nat. Biotechnol.*, **28**, 1045–1048.
45. Robinson,J.T., Thorvaldsdottir,H., Winckler,W., Guttman,M., Lander,E.S., Getz,G. and Mesirov,J.P. (2011) Integrative genomics viewer. *Nat. Biotechnol.*, **29**, 24–26.
46. Anders,S., Pyl,P.T. and Huber,W. (2015) HTSeq–a python framework to work with high-throughput sequencing data. *Bioinformatics*, **31**, 166–169.
47. Dobin,A., Davis,C.A., Schlesinger,F., Drenkow,J., Zaleski,C., Jha,S., Batut,P., Chaisson,M. and Gingeras,T.R. (2013) STAR: ultrafast universal RNA-seq aligner. *Bioinformatics*, **29**, 15–21.
48. Bray,N.L., Pimentel,H., Melsted,P. and Pachter,L. (2016) Near-optimal probabilistic RNA-seq quantification. *Nat. Biotechnol.*, **34**, 525–527.
49. Love,M.I., Huber,W. and Anders,S. (2014) Moderated estimation of fold change and dispersion for RNA-seq data with DESeq2. *Genome Biol.*, **15**, 550.
50. Babicki,S., Arndt,D., Marcu,A., Liang,Y., Grant,J.R., Maciejewski,A. and Wishart,D.S. (2016) Heatmapper: web-enabled heat mapping for all. *Nucleic Acids Res.*, **44**, W147–W153.
51. Gusev,Y., Bhuvaneshwar,K., Song,L., Zenklusen,J.-C., Fine,H. and Madhavan,S. (2018) The REMBRANDT study, a large collection of genomic data from brain cancer patients. *Sci. Data*, **5**, 180158.
52. Zhao,Z., Zhang,K.N., Wang,Q., Li,G., Zeng,F., Zhang,Y., Wu,F., Chai,R., Wang,Z., Zhang,C. *et al.* (2021) Chinese glioma genome atlas (CGGA): a comprehensive resource with functional genomic data from chinese glioma patients. *Genomics Proteomics Bioinformatics*, **19**, 1–12.
53. Bowman,R.L., Wang,Q., Carro,A., Verhaak,R.G. and Squatrito,M. (2017) GlioVis data portal for visualization and analysis of brain tumor expression datasets. *Neuro-oncol.*, **19**, 139–141.
54. Subramanian,A., Tamayo,P., Mootha,V.K., Mukherjee,S., Ebert,B.L., Gillette,M.A., Paulovich,A., Pomeroy,S.L., Golub,T.R., Lander,E.S. *et al.* (2005) Gene set enrichment analysis: a knowledge-based approach for interpreting genome-wide expression profiles. *Proc. Natl. Acad. Sci. U.S.A.*, **102**, 15545–15550.
55. Gilbert,J.A., Skrzynski,M.C. and Lester,G.E. (1989) Cross-sectional moment of inertia of the distal radius from absorptiometric data. *J. Biomech.*, **22**, 751–754.
56. Huang da,W., Sherman,B.T. and Lempicki,R.A. (2009) Systematic and integrative analysis of large gene lists using DAVID bioinformatics resources. *Nat. Protoc.*, **4**, 44–57.
57. Huang da,W., Sherman,B.T. and Lempicki,R.A. (2009) Bioinformatics enrichment tools: paths toward the comprehensive functional analysis of large gene lists. *Nucleic Acids Res.*, **37**, 1–13.
58. Kanehisa,M., Furumichi,M., Tanabe,M., Sato,Y. and Morishima,K. (2017) KEGG: new perspectives on genomes, pathways, diseases and drugs. *Nucleic Acids Res.*, **45**, D353–D361.
59. Abounader,R. and Laterra,J. (2005) Scatter factor/hepatocyte growth factor in brain tumor growth and angiogenesis. *Neuro-oncol.*, **7**, 436–451.
60. Koochekpour,S., Jeffers,M., Rulong,S., Taylor,G., Klineberg,E., Hudson,E.A., Resau,J.H. and Vande Woude,G.F. (1997) Met and hepatocyte growth factor/scatter factor expression in human gliomas. *Cancer Res.*, **57**, 5391–5398.
61. Huang,W., Liu,H. and Lv,T. (2021) Silencing of SETD6 inhibits the tumorigenesis of oral squamous cell carcinoma by inhibiting methylation of PAK4 and relA. *Histol. Histopathol.*, **36**, 229–237.
62. Peixoto,P., Etcheverry,A., Aubry,M., Missey,A., Lachat,C., Perrard,J., Hendrick,E., Delage-Mourroux,R., Mosser,J., Borg,C. *et al.* (2019) EMT is associated with an epigenetic signature of ECM remodeling genes. *Cell Death. Dis.*, **10**, 205.
63. Iser,I.C., Lenz,G. and Wink,M.R. (2019) EMT-like process in glioblastomas and reactive astrocytes. *Neurochem. Int.*, **122**, 139–143.
64. Iser,I.C., Pereira,M.B., Lenz,G. and Wink,M.R. (2017) The Epithelial-to-Mesenchymal transition-like process in glioblastoma: an updated systematic review and in silico investigation. *Med. Res. Rev.*, **37**, 271–313.
65. Gonzalez,D.M. and Medici,D. (2014) Signaling mechanisms of the epithelial-mesenchymal transition. *Sci. Signal*, **7**, re8.
66. Myung,J.K., Choi,S.A., Kim,S.K., Wang,K.C. and Park,S.H. (2014) Snail plays an oncogenic role in glioblastoma by promoting epithelial mesenchymal transition. *Int. J. Clin. Exp. Pathol.*, **7**, 1977–1987.
67. Singh,S. and Gramolini,A.O. (2009) Characterization of sequences in human TWIST required for nuclear localization. *BMC Cell Biol.*, **10**, 47.
68. Kublanovsky,M., Aharoni,A. and Levy,D. (2018) Enhanced PKMT-substrate recognition through non active-site interactions. *Biochem. Biophys. Res. Commun.*, **501**, 1029–1033.
69. Feldman,M. and Levy,D. (2018) Peptide inhibition of the SETD6 methyltransferase catalytic activity. *Oncotarget*, **9**, 4875–4885.
70. Wang,X., Wang,Y., Xie,F., Song,Z.T., Zhang,Z.Q., Zhao,Y., Wang,S.D., Hu,H., Zhang,Y.S. and Qian,L.J. (2022) Norepinephrine promotes glioma cell migration through up-regulating the expression of twist1. *BMC Cancer*, **22**, 213.
71. Cai,X., Feng,S., Zhang,J., Qiu,W., Qian,M. and Wang,Y. (2020) USP18 deubiquitinates and stabilizes twist1 to promote epithelial-mesenchymal transition in glioblastoma cells. *Am J Cancer Res*, **10**, 1156–1169.
72. Binda,O. (2020) Lysine methyltransferase SETD6 modifies histones on a glycine-lysine motif. *Epigenetics*, **15**, 26–31.
73. Han,X., Liu,J., Liu,Y., Mou,L. and Li,C. (2021) LINC-PINT inhibited malignant progression of bladder cancer by targeting miR-155-5p. *Cancer Manag. Res.*, **13**, 4393–4401.
74. Hao,T., Huang,S. and Han,F. (2020) LINC-PINT suppresses tumour cell proliferation, migration and invasion through targeting miR-374a-5p in ovarian cancer. *Cell Biochem. Funct.*, **38**, 1089–1099.
75. Xie,Z., Bailey,A., Kuleshov,M.V., Clarke,D.J.B., Evangelista,J.E., Jenkins,S.L., Lachmann,A., Wojciechowicz,M.L., Kropiwnicki,E., Jagodnik,K.M. *et al.* (2021) Gene set knowledge discovery with enrichr. *Curr. Protoc.*, **1**, e90.
76. Kuleshov,M.V., Jones,M.R., Rouillard,A.D., Fernandez,N.F., Duan,Q., Wang,Z., Koplev,S., Jenkins,S.L., Jagodnik,K.M., Lachmann,A. *et al.* (2016) Enrichr: a comprehensive gene set enrichment analysis web server 2016 update. *Nucleic Acids Res.*, **44**, W90–W97.
77. Chen,E.Y., Tan,C.M., Kou,Y., Duan,Q., Wang,Z., Meirelles,G.V., Clark,N.R. and Ma'ayan,A. (2013) Enrichr: interactive and collaborative HTML5 gene list enrichment analysis tool. *BMC Bioinf.*, **14**, 128.
78. Sloan,C.A., Chan,E.T., Davidson,J.M., Malladi,V.S., Strattan,J.S., Hitz,B.C., Gabdank,I., Narayanan,A.K., Ho,M., Lee,B.T. *et al.* (2016) ENCODE data at the ENCODE portal. *Nucleic Acids Res.*, **44**, D726–D732.
79. Margueron,R., Li,G., Sarma,K., Blais,A., Zavadil,J., Woodcock,C.L., Dynlacht,B.D. and Reinberg,D. (2008) Ezh1 and ezh2 maintain repressive chromatin through different mechanisms. *Mol. Cell*, **32**, 503–518.
80. Cao,R., Wang,L., Wang,H., Xia,L., Erdjument-Bromage,H., Tempst,P., Jones,R.S. and Zhang,Y. (2002) Role of histone H3 lysine 27 methylation in Polycomb-group silencing. *Science*, **298**, 1039–1043.
81. Patterson,R.P. (1987) Possible technique to measure ventricular volume using electrical impedance measurements with an oesophageal electrode. *Med. Biol. Eng. Comput.*, **25**, 677–679.
82. Cakouros,D., Isenmann,S., Cooper,L., Zannettino,A., Anderson,P., Glackin,C. and Gronthos,S. (2012) Twist-1 induces ezh2 recruitment regulating histone methylation along the ink4a/arf locus in mesenchymal stem cells. *Mol. Cell. Biol.*, **32**, 1433–1441.
83. Rahme,G.J. and Israel,M.A. (2015) Id4 suppresses MMP2-mediated invasion of glioblastoma-derived cells by direct inactivation of twist1 function. *Oncogene*, **34**, 53–62.
84. Jacqueroud,L., Bouard,C., Richard,G., Payen,L., Devouassoux-Shisheboran,M., Spicer,D.B., Caramel,J., Collin,G., Puisieux,A., Tissier,A. *et al.* (2016) The heterodimeric TWIST1-E12 complex drives the oncogenic potential of TWIST1 in human mammary epithelial cells. *Neoplasia*, **18**, 317–327.

Downloaded from https://academic.oup.com/nar/advance-article/doi/10.1093/nar/gkac485/6606173 by Ben Gurion University of the Negev-Medical Library user on 15 June 2022

85. Zhang,W.J., Wu,X.N., Shi,T.T., Xu,H.T., Yi,J., Shen,H.F., Huang,M.F., Shu,X.Y., Wang,F.F., Peng,B.L. *et al.* (2016) Regulation of transcription factor yin yang 1 by SET7/9-mediated lysine methylation. *Sci. Rep.*, **6**, 21718.
86. Ea,C.K. and Baltimore,D. (2009) Regulation of NF-kappaB activity through lysine monomethylation of p65. *Proc. Natl. Acad. Sci. U.S.A.*, **106**, 18972–18977.
87. Chuikov,S., Kurash,J.K., Wilson,J.R., Xiao,B., Justin,N., Ivanov,G.S., McKinney,K., Tempst,P., Prives,C., Gamblin,S.J. *et al.* (2004) Regulation of p53 activity through lysine methylation. *Nature*, **432**, 353–360.
88. Vershinin,Z., Feldman,M. and Levy,D. (2020) PAK4 methylation by the methyltransferase SETD6 attenuates cell adhesion. *Sci. Rep.*, **10**, 17068.
89. Banyard,J. and Bielenberg,D.R. (2015) The role of EMT and MET in cancer dissemination. *Connect. Tissue Res.*, **56**, 403–413.
90. Janiszewska,M., Primi,M.C. and Izard,T. (2020) Cell adhesion in cancer: beyond the migration of single cells. *J. Biol. Chem.*, **295**, 2495–2505.
91. De Pascalis,C. and Etienne-Manneville,S. (2017) Single and collective cell migration: the mechanics of adhesions. *Mol. Biol. Cell*, **28**, 1833–1846.
92. Matsuo,N., Shiraha,H., Fujikawa,T., Takaoka,N., Ueda,N., Tanaka,S., Nishina,S., Nakanishi,Y., Uemura,M., Takaki,A. *et al.* (2009) Twist expression promotes migration and invasion in hepatocellular carcinoma. *BMC Cancer*, **9**, 240.
93. Yang,H., Cao,C. and Wang,L.J. (2020) [LncRNA LINC-PINT regulating proliferation and apoptosis of osteosarcoma cells by targeting miR-524-5p]. *Zhonghua Zhong Liu Za Zhi*, **42**, 325–330.
94. Chau,Y.K., Zhang,S. and Maguire,R.J. (1992) Determination of butyltin species in sewage and sludge by gas chromatography-atomic absorption spectrometry. *Analyst*, **117**, 1161–1164.
95. Porter,J.M., Sussman,M.S. and Rosen,G.M. (1988) Cocaine-induced hepatotoxicity. *Hepatology*, **8**, 1713.

Downloaded from https://academic.oup.com/nar/advance-article/doi/10.1093/nar/gkac485/6606173 by Ben Gurion University of the Negev-Medical Library user on 15 June 2022